LOW CARBON LIVING CRC

RP1037u1: Above-Roof Temperature Impacts on Heating Penalties of Large Cool Roofs in Australian Climates

Final Report

Authors	Wenye Lin, Alan Green, Georgios Kokogiannakis and Paul Cooper
Title	Above-Roof Temperature Impacts on Heating Penalties of Large Cool Roofs in Australian Climates – Interim Report 2
ISBN	
Date	17/6/2019
Keywords	Cool roof, Dew, Condensation, Building energy performance, Sustainability, cost-benefit analysis
Publisher	
Preferred citation	

Australian Government
Department of Industry, Innovation and Science
Business Cooperative Research Centres Programme

Acknowledgements

The authors would like to acknowledge the contributions of Bluescope Steel, especially the ongoing involvement of Mark Eckermann and Jamie Adams in the project. We would also like to recognise contributions made to the previous stage of this project, which formed a basis for much of the work contained in this report, by our colleagues at the University of New South Wales: Riccardo Paolini, Shamila Haddad, Afroditi Synnefa, Mattheos Santamouris and Baojie Hek, and at the University of Wollongong: Laia Ledo Gomis, Ben Zeitsch, David Beecher, Zhenjun Ma and Buyung Kosasih.

This research was funded by the CRC for Low Carbon Living Ltd supported by the Cooperative Research Centres program, an Australian Government initiative.

Disclaimer

Any opinions expressed in this document are those of the authors. They do not purport to reflect the opinions or views of the CRCLCL or its partners, agents or employees.

The CRCLCL gives no warranty or assurance, and makes no representation as to the accuracy or reliability of any information or advice contained in this document, or that it is suitable for any intended use. The CRCLCL, its partners, agents and employees, disclaim any and all liability for any errors or omissions or in respect of anything or the consequences of anything done or omitted to be done in reliance upon the whole or any part of this document.

Peer Review Statement

The CRCLCL recognises the value of knowledge exchange and the importance of objective peer review. It is committed to encouraging and supporting its research teams in this regard.

The authors confirm that this document has been reviewed and approved by the project's program leader and steering committee. The program leader provided constructive feedback, which has been addressed.

Contents

List of Tables

List of Figures

Acronyms

BPS	Building performance simulation
CFD	Computational fluid dynamics
COP	Coefficient of performance
EMS	Energy management system
HVAC	Heating, ventilation and air-conditioning
IWEC	International Weather for Energy Calculation
NCC2019	Australian national construction code 2019
PV	Photovoltaic
RMS	Root-mean square
RMSE	Root-mean square error
RP1037	The preceding project ‘Driving increased utilisation of cool roofs on large-footprint buildings’
RP1037u1	The current project ‘Above-Roof Temperature Impacts on Heating Penalties of Large Cool Roofs in Australian Climates’
UDF	User-defined function

Executive Summary

This report outlines the key outcomes of research project RP1037u1 'Above-Roof Temperature Impacts on Heating Penalties of Large Cool Roofs in Australian Climates', an extension to project RP1037 'Driving increased utilisation of cool roofs on large-footprint buildings'. The research has been focused on two key aspects of roof thermal performance that had, up until the time of writing, not been taken into account in most investigations into cool roof technology:

1. The condensation and evaporation of dew on the roof surface, and the effect this has on roof temperature by way of:
    a. The latent heat that is absorbed and released; and
    b. Any change in the effective radiative-optical properties of the roof top surface due to accumulated water.
2. The effect of roof temperature on above-roof air temperatures, and the influence this can have on the performance of rooftop heating, ventilation and air-conditioning (HVAC) equipment.

A review of relevant literature (included in this report) did not reveal any previous studies that had investigated both 1a and 1b, above. Previous experimental studies had shown that the apparent thermal emittance of surfaces can approach ~0.96 when covered in a film of water. The surface temperature of low-emittance roofing materials, e.g. metal-coated steel, could be influenced significantly by such a change in emittance. Furthermore, experimental data from RP1037 revealed that roof surface temperatures often fell below the dew-point temperature at night and during the early morning, which confirmed that roof surfaces were likely to often be wet with dew.

A roof condensation model was developed from fundamental thermodynamic principles and previously established sub-models, to quantify the effect that water condensation can have on roof temperatures. When implemented in a dynamic building performance simulation (BPS), the model predicts the latent heat flux introduced by dew condensation and evaporation, tracks the accumulation of a dew film on the roof, and calculates the roof surface apparent thermal emittance, taking into account the effect of the dew.

The above-roof temperature model, developed based on experimental data in RP1037, has also been revised in the present work. The model can be used to predict the actual temperature of air entering rooftop HVAC equipment in BPS, taking into account the effect of the roof surface temperature, wind, and height of the HVAC inlet duct. Both new models (the roof condensation model and revised above-roof temperature model) have been described in this report, and summarised guides on how to implement the models in simulations have also been provided for BPS practitioners.

To test the effects of dew and above-roof temperatures on a case-study 350×200 m^2 two-storey shopping centre building, a parametric BPS study was conducted. Simulations were run of seven Australian climate zones, three roof types (one bare metal-coated steel roof, one light-coloured painted steel roof, and one even lighter cool roof), two HVAC systems, and four thicknesses of ceiling insulation. Each simulation was run four times: i) with the revised above-roof temperature model, ii) with the roof condensation model, iii) with neither model, and iv) with both models.

A comparison of simulation results indicated that rooftop dew and above-roof air temperature fields can affect BPS results significantly, especially in cases where multiple simulations are being compared to assess the relative effects of cool roofs. If both phenomena had been neglected in the cases investigated here, electricity savings would have been miscalculated by 11–75% (42% on average) and gas 'penalties' (i.e. extra gas consumption for heating of the building) would have been miscalculated by 16–46% (31% on average). When both models were implemented, calculated gas penalties attributable to the cool roof were consistently reduced and HVAC electricity savings were either reduced or increased, depending on the climate.

The operational and emissions savings attributable to cool roofs depend on the unit costs and greenhouse gas emission factors of electricity and gas, so a range of unit costs and emission factors were investigated in the economic analysis. Compared to the bare-metal roof, the cool roof provided a net saving in HVAC running costs and reduction in greenhouse gas emissions for the case-study building in almost all cases involving Darwin, Brisbane, Alice Springs and Sydney. In simulations of Dubbo, Melbourne and Canberra, running costs and emissions could be reduced or increased by the cool roof, depending on the unit costs and emission factors.

The net effect of rooftop dew and above-roof air temperature fields on predicted HVAC running cost savings and greenhouse gas emissions abatements for the cool roof varied, but was generally positive. When both models were implemented, the predicted cool roof benefits were consistently increased in simulations of Dubbo, Sydney, Melbourne and Canberra. In hotter climates (Darwin, Brisbane and Alice Springs), the combined effects of dew and above-roof temperatures were found to either increase or decrease the predicted cool roof benefits, depending on the emission factors and unit costs of electricity and gas.

The case-studies reported here demonstrate the large effect that above-roof temperature fields and dew can have on simulation studies of this type. The two models developed here will allow BPS practitioners to account for such effects in future investigations. Further research into several aspects of the phenomena would be valuable, including:

- Further validation of the above-roof temperature model, in a wider range of weather conditions and on different types of building;
- Investigation into the effects of uneven dew film coverage; and
- Extension of the BPS parametric study to include more buildings and climates.

Introduction

Background

'Cool' roofing materials are engineered to maximise the solar reflectance and thermal emittance of the roof top surface. Cool roofs tend to remain colder than those fabricated from conventional roofing materials, because they reflect a relatively large fraction of incoming short-wave solar radiation, and transmit a relatively large quantity of long-wave radiation to the sky (as compared to low-emissivity bare metal roofs). Such a reduction in surface temperature can reduce the amount of heat transmitted into a building during hot periods, thereby reducing the energy required for space cooling and/or improving the indoor comfort conditions. However, in cold conditions cool roofs tend to reduce indoor thermal comfort and/or increase the energy required to heat indoor spaces—an effect often referred to as the cool roof 'heating penalty'. Thus, the suitability of cool roof technology depends on the local climate, as well as the building design and usage.

A recently completed research project entitled 'Driving Increased Utilisation of Cool Roofs on Large-Footprint Buildings' (RP1037) investigated previous claims that cool roofs may have additional effects on the performance of buildings with large roof surfaces (e.g. airport terminals and shopping centres) and rooftop heating, ventilation and air-conditioning (HVAC) equipment (Green *et al.*, 2018). In that study, it was confirmed experimentally that, in addition to the effects that cool roofs have on heat transmission through the roof structure, they can also significantly alter the temperature of air surrounding rooftop HVAC equipment. An empirical model was formed that can predict near-roof air temperatures, taking into account the influence of roof surface temperature, and the model was implemented in a set of building performance simulations (BPS). The simulation results indicated that the effect roof surface temperatures have on ventilation air inlet temperatures and rooftop heat exchanger efficiencies can cause changes in annual HVAC electricity and gas consumption of up to 5%. Moreover, in the cases investigated, these above-roof air temperature effects were found to account for approximately half of the benefits and penalties associated with cool roofs. Thus, if the near-roof air temperature field had not been modelled accurately (as is currently the conventional practice in BPS), the cooling savings and heating penalties associated with cool roofs would have been underestimated by approximately 50%.

The findings of RP1037 have provided valuable insights into the magnitude of effect that near-roof air temperatures can have, and the importance of these effects in the performance of cool roofs. The empirical above-roof temperature model has also provided a means for BPS practitioners to take near-roof air temperatures into account. However, the experiments on which the model was based were limited to three buildings and a relatively small set of weather conditions. Therefore, validation of the model with additional experimental data would be highly valuable, and users of the model should have a clear understanding of any limits to the range of conditions which it is valid for. In particular, the validity of the model for use in simulations of cold conditions is of interest, since the experiments were all conducted in warm summer/autumn conditions and the model has a large effect on predicted cool roof heating penalties, which arise in cold conditions. This issue has been investigated in the present work.

The second issue that has been investigated in the research reported here is that of water condensation on roof surfaces, and the effects that this phenomenon can have on the performance of cool roofs relative to roofs constructed of more conventional roofing materials. When a roof surface temperature falls below the local dew-point temperature, water will condense on the surface, which could have two potentially significant effects on the thermal performance of roofing materials:

1. The release of latent heat during condensation and absorption of latent heat during evaporation could significantly influence roof surface temperatures.
2. Water droplets or films on the roof surface could significantly alter the roof radiative-optical properties, thereby influencing roof surface temperatures.

Prior to investigation, it was speculated that cool roofs and 'non-cool' roofs could reach very similar temperatures when covered in condensed water, and that this could significantly reduce cool roof heating penalties. In the present study, the authors have quantified the effects of condensation on cool and 'non-cool' roofs, in order to determine whether this could be true.

Aims

The aims of the current project are outlined below:

1. Quantify the range of weather conditions for which the existing RP1037 above-roof temperature model can be applied, and develop a new model for cold weather conditions if needed.
2. Quantify the effects of condensation on cool roof thermal performance, relative to metal-coated ('non-cool') roofing materials.
3. Revise results from the RP1037 BPS, cost-benefit analysis and greenhouse gas emissions abatement calculations, to take into account any revisions to the above-roof temperature model, and the effects of condensation if they prove to be significant.
4. Ensure utilisation of research outcomes by producing technical design support resources, conducting a series of seminars for key user groups, and disseminating findings in appropriate industry and academic publications.

Method

The project has been divided into four primary activities:

1. Investigate the effects of condensation on cool roof performance, by:

a. reviewing literature related to condensation on roofs and the physical phenomena involved in this process;

b. analysing the existing RP1037 dataset, to determine how often condensation was likely to occur and whether there was a discernible effect on roof surface temperatures at those times;

c. developing a model that can estimate the rate of water condensation and evaporation on a roof surface, as well as the effects of these processes on roof radiative-optical properties and the roof temperature; and

d. conducting dynamic BPS, with and without the condensation model, of buildings with cool and 'non-cool' bare metal-coated steel roofs, to quantify the effect of condensation in several illustrative cases.

2. Address issues related to use of the existing above-roof temperature model in simulations of cold conditions, by:

   a. quantifying the range of weather conditions recorded during the RP1037 experiments and comparing this to the range of conditions predicted throughout a typical year in different Australian climates; and

   b. revising the above-roof temperature model if necessary.

3. Replicate BPS, cost-benefit analysis and greenhouse gas emissions abatement calculations from RP1037, incorporating the condensation model and revised above-roof temperature model, if necessary.

4. Disseminate research findings through publications, seminars, and summary design support resources.

Report outline

Key outcomes from the activities outlined above have been included in this report, organised into six sections:

1. Literature review.
2. Condensation likelihood based on the RP1037 dataset.
3. Roof condensation model definition and assessment.
4. Investigation into dew runoff flow from roofs.
5. Above-roof temperature model definition and assessment.
6. Updated building performance simulations, including both new models.
7. Cost-benefit and greenhouse gas emissions analyses, based on updated BPS results.

Summarised guidelines for the implementation of the two new models in BPS have also been included, as appendices to this report.

Literature Review

A review has been presented here, of the potential influences that dew may have on roof thermal performance, and different approaches to quantify these influences. First, previous investigations into water condensation on roofs are discussed, then the two primary mechanisms by which dew can effect roof thermal performance are explored in more detail, namely: i) latent heat release/absorption during the condensation and evaporation processes, and ii) changes in the apparent radiative-optical properties of the roof surface.

Previous work on roof condensation

A number of previous studies have investigated water condensation on roofs. Some of these studies investigated condensation inside the roof cavity, on the internal surface of the roof (Simpson *et al.*, 1992; Essah *et al.*, 2009). Depending on the roof construction and internal conditions, water can condense indoors or between layers of the roof system. Condensation on the roof top/external surface (i.e. dew formation) is influenced only by the outdoor conditions and roof surface temperature. Studies into internal condensation have not been discussed in-detail in this report, and the present study was focused on dew formation on the external roof surface.

A small number of previous studies have investigated water condensation on roof external surfaces (Pieters *et al.*, 1995; Tywoniak, 1999; Richards, 2009; Piscia *et al.*, 2012). Of these studies, it appears that none have taken into account the effect of water droplets and films on roof radiative-optical properties. Furthermore, most of these previous investigations arguably did not adopt the most appropriate convective heat transfer coefficient algorithms for use on roof-like surfaces. Convective heat transfer coefficients are used to calculate mass transfer coefficients, which directly influence calculated condensation and evaporation rates, and thereby, latent heat release/absorption rates. Therefore, the two key effects of dew on roof thermal performance, the heat fluxes caused by the latent heat release and absorption, and changes in radiative-optical properties, may not have been modelled accurately. These previous investigations have been summarised briefly below.

Richards (2009) adapted an existing model, designed to estimate dew accumulation on leaves for the agricultural sector, into an urban dew model for estimation of the quantity of dew that could be harvested from roof surfaces. One of the empirical models from Mcadams (1942) was used to calculate the convective heat transfer coefficient, and thereby predict the latent heat transfer. The emissivity of the roof surface was not modified to account for the effects of dew. Comparison of the model results with experimental data revealed a RMS error of 0.04 mm in terms of the dew thickness accumulated over night, which was significant considering that the mean end-of-night dew thickness was 0.09 mm. One source of error is likely to have been the convective heat transfer model used, which is only applicable for wind speeds lower than 5 m s^{-1}.

Tywoniak (1999) studied water condensation on cold roof surfaces numerically. Dew deposition was allowed on both the internal and external roof surfaces, under the assumption that the sub-roof space was well ventilated (i.e. had equal temperature and humidity as the outdoor space). The release/absorption of latent heat was calculated using a model from Bloudek (1992). However, a convective heat transfer model was adopted that is only applicable to free convection (i.e. conditions with negligible wind). Furthermore, the effects of dew on the apparent emissivity of the roof surfaces were not considered. The model predicted an extremely high total condensation rate.

Piscia *et al.* (2012) carried out computational fluid dynamics (CFD) simulations, to predict the indoor conditions of a greenhouse, taking into account the effects of condensation on the greenhouse roof. A user-defined function (UDF) was coupled with a commercial CFD package to simulate the film condensation. However, the apparent emissivity of the roof surface was not modified to account for the effects of dew. The results showed that the condensation rate could be represented quite accurately by a logistic function regression, which would vary according to the conditions. However, the CFD results were only validated in terms of the greenhouse indoor conditions, and no evidence was presented that supported the accuracy of simulated dew condensation. Furthermore, the simulation was carried out for a four-span greenhouse roof with a roof pitch of 45º, so the results cannot necessarily be applied directly to large, near-horizontal, opaque roofs.

Pieters *et al.* (1995) modelled the onset of condensation on both the inner and outer surfaces of greenhouse covers. It was found that the use of low emissivity glass can increase the threshold of condensation for both inner and outer surfaces of a greenhouse. However, the modelling was not continued, to investigate the effects of water condensation on the roof thermal performance after condensation had started to form. The convective heat transfer coefficient that was used was not specified.

Latent heat

As water condenses on roof surfaces, it releases latent heat, and as it evaporates, it absorbs the same amount of latent heat. The quantity of latent energy that is released/absorbed per unit mass of water is a well-known quantity referred to the specific heat of vaporisation; it is equal to approximately 2,257 kJ kg^{-1} at atmospheric pressure (Çengel and Boles, 2002). Therefore, if the dew mass transfer rate can be accurately quantified, the significance of latent heat effects on the thermal performance of roofs can be evaluated.

In the BPS software EnergyPlus (EnergyPlus, 2010), an optional setting is available to take into account the latent heat effects of condensation on building external surfaces, without calculating the mass transfer rate. In this approach, an extremely high convective heat transfer coefficient is set for any surface that is below the dew-point temperature, and the outdoor air temperature applied to that surface is artificially set to the dew-point temperature. Thus, external surface temperatures are prevented from falling significantly below the dew-point

temperature. Inherent in this approach are assumptions that: i) the mass transfer rate during condensation is effectively unlimited, so that sufficient latent heat can be released to maintain the surface at the dew-point temperature, and ii) the evaporation process does not have a significant effect surface temperatures. No justification was found in the EnergyPlus documentation for either of these assumptions, and no other evidence was uncovered in this review that appears to justify them.

Some studies have estimated evaporation/condensation rates by performing a statistical regression on experimental data. For instance, a series of regression models were proposed by Maestre-Valero *et al.* (2015) and Beysens *et al.* (2006) to predict dew formation on various surfaces, given different ambient conditions. However, the simplicity of these models was shown to produce considerable errors in predictions of dew accumulation rates (R^2 ranging from 0.27 to 0.57) (Maestre-Valero *et al.*, 2015).

Condensation and evaporation rates can also be deduced theoretically, based on an analogy between convective heat and mass transfer. It has been demonstrated experimentally that these two related processes can be correlated using the Lewis number (Bergman *et al.*, 2011). Thus, if the convective heat transfer coefficient can be estimated accurately, it can be used to calculate the convective mass transfer coefficient (Tiwari *et al.*, 1982; Keller, 1985; Beysens *et al.*, 2005; Richards, 2009; Monteith and Unsworth, 2013). Therefore, it is important that a convective heat transfer coefficient correlation that is accurate for roofs is used, if accurate condensation/evaporation estimates are to be attained via this method.

Many correlations have been recommended for the estimation of convective heat transfer at the external surfaces of buildings, and several researchers have compared them (Mirsadeghi *et al.*, 2013; Costanzo *et al.*, 2014). Many of the correlations were based on laboratory-scale experiments and have not been validated for building-scale surfaces, so it is unclear whether they are valid for such large length scales. Furthermore, the 'completeness' of the different correlations, in terms of the set of relevant physical factors that they take into account (e.g. surface orientation, surface size, surface roughness, air flow turbulence characteristics, roof/air temperature difference, etc.), varies widely. A selection of the most relevant correlations have been described below.

Duffie and Beckman (2013) presented a range of convective heat transfer correlations, but recommended one model, based on work by Mitchell (1976), for use on large building-scale surfaces in outdoor conditions. This model combines an empirical correlation for forced convection conditions with a minimal value of 5 W m^{-2} K^{-1} which applies to natural convection as long as the wind speed is lower than 5 m s^{-1}.

Mirsadeghi *et al.* (2013) summarised and compared a number of external convective heat transfer coefficient models that were in common use in BPS programs. The most 'complete' models were the 'BLAST'-related models (including the 'TARP' model), the 'MoWitt' model and the 'DOE-2' model. However, the BLAST-related models do not appear to have been thoroughly validated for building-scale surfaces, and the MoWitt model was developed based on vertical building surfaces, so may not be valid for roofs.

A convective heat transfer model developed by Krisher and Kast (which was used by Holck and Svendsen (2004) for latent heat flux calculation) takes the difference between laminar and turbulent flow into account. The 'completeness' of this model was high; however, the range of applicability of this model was not clearly stated.

Costanzo *et al.* (2014) compared a number of commonly used convective heat transfer coefficient models to field measurements from a flat roof in Italy. Results obtained using the different models deviated from each other considerably. The 'ClearRoof' model, proposed by Clear *et al.* (2003), reproduced the experimental data most accurately, followed by the TARP model.

Of the models reviewed here, the ClearRoof model is one of the most 'complete'. Furthermore, it was developed for use in relation to the horizontal roofs of commercial buildings, and further validated for such surfaces by Costanzo *et al.* (2014). It is not clear to the present authors whether the treatment, within the ClearRoof model, of above-roof air flow as laminar when the reference wind speed is below a certain threshold is valid, since the sharp leading edge of the roof surface is likely to 'trip' flow into a turbulent state. This has been documented in many studies of air flow around buildings (Castro and Robins, 1977; Richards *et al.*, 2007; Blocken *et al.*, 2013). Nevertheless, the ClearRoof model has accurately reproduced two sets of experimental results from full-scale flat-roofed buildings in real wind, so it appears to be one of the most suitable models available for such cases.

Influence on radiative-optical properties

Thermal emittance

It has been reported in a number of studies that the presence of water droplets or films on a surface can influence the long-wave radiant heat transfer to/from the surface significantly (Lee *et al.*, 2016). Robinson *et al.* (1957) used a guarded hot box to measure changes in the thermal resistance of a reflective foil surface as water condensed on the surface. When condensed water was observed to cover approximately 10% of the foil area, the foil thermal resistance was reduced by 10-30%. They attributed the phenomenon to the high emittance of water film, even when it was only a few thousandths of an inch thick.

Bassett and Trethowen (1984) also investigated the effect of condensed water on the emittance of reflective insulation surfaces. They found that condensate loadings of 1 g m^{-2} (1 µm mean thickness) increased the apparent emittance of aluminium foil from 0.06 to 0.25. It was noted that the apparent emittance did not immediately rise to that of a bulk water when water was present, but increased gradually with increasing condensate thickness. This could be explained by the infrared transmittance of a water film being non-zero (i.e. while water is a strong absorber in the infrared, it is not entirely

opaque). It was also observed that, when the condensate mass loading was maintained at 0.92 and 0.55 g m^{-2} over a period of more than 5 days, the apparent emissivity decreased slightly within the first 24 h (by 0.03 and 0.15, respectively), but afterwards little change was observed. It was suggested that this change could have been caused by droplet coalescence, which would alter the fraction of the surface that is covered by water and the depth of the water layer.

Mao and Kurata (1998) conducted experiments into the influence of condensation on the thermal performance of porous sheets used to cover agricultural crops. The results revealed that the apparent emissivity of the row cover materials increased from 0.26 to approximately 0.45, given dew deposition of 0-40 g m^{-2}.

Ambrose and Karagiozis (2007) numerically evaluated the thermal benefits of using a pressure-equalized insulated glass unit (IGU) in building envelopes. In the simulations, the effect of condensed water on the apparent emissivity of glass panes with low-emission coatings was modelled using outcomes from the experiments carried out by Bassett and Trethowen (1984). It is possible that a similar approach can be taken in the investigation of roof surfaces.

Solar reflectance

It has been reported that the solar (i.e. short-wave) reflectance of glazed photovoltaic panels at a perpendicular incidence angle can be about 4-5%, due to the high refractive index of the glass layers (Krauter, 2004). Similarly, when dew exists on a roof surface, it acts as a reflective layer. However, since water has a lower refractive index than glass, 1.33 vs. ~1.5 (Hosseini *et al.*, 2019), the reflection loss is smaller. According to the Fresnel equation, the solar reflectance of a water film at a perpendicular incidence angle is around 2–3%.

Surface soiling

It has been suggested that dew can cause dust to accumulate on roof surfaces, thereby gradually changing the roof surface radiative-optical properties over time (Ilse *et al.*, 2019). As was identified in RP1037, the soiling of roof surfaces can affect their thermal performance significantly. However, it is likely that any contribution dew has in the ageing/fouling of roofing materials is already accounted for in the empirical models used to predict these effects (Sleiman *et al.*, 2011, 2014; Paolini *et al.*, 2014).

Condensation likelihood in the RP1037 dataset

Experimental data collected in RP1037 includes over 18 weeks of roof surface temperature and local dew-point temperature measurements. Three case study shopping centres were studied; roof surface temperatures were measured at 15 locations on each roof and the dew-point temperature was measured at the top of an 8m-tall mast, near the centre of each roof. While condensation was not measured directly, any measured roof surface temperature equal to, or lower than, the corresponding dew-point temperature indicates that roof condensation was likely at that time.

The spatially averaged roof surface temperature, T_s, dropped below the dew-point temperature, T_{dp}, on approximately 80% of nights, at each of the three buildings studied (see an example of a typical 24 h period in Figure 1 and a summary of all measurements in Figure 2). When this occurred, T_s often reached temperatures several degrees below T_{dp}, for several hours. Two conclusions can be drawn from these observations: i) water is likely to have condensed on the roof surfaces on most nights during the monitoring periods, and ii) the latent heat released during the condensation process was insufficient to keep the roof surface temperatures at or above the dew-point temperature. Whether or not the condensed water had a significant effect on roof surface temperatures cannot be determined from the RP1037 dataset alone, so a new condensation model has been developed and applied in the subsequent sections of this report, to quantify such effects.

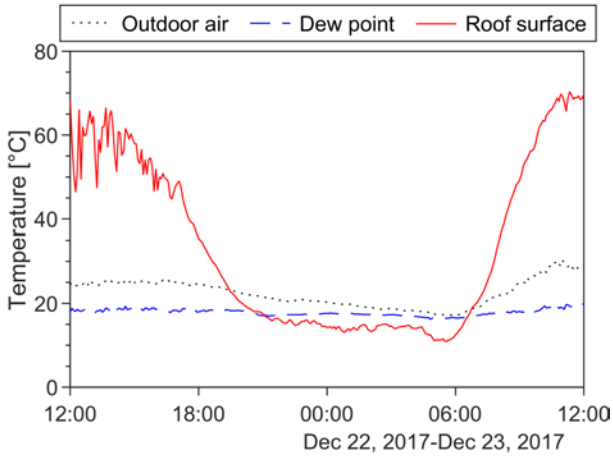

Figure 1: Comparison of outdoor air, dew point and spatially averaged roof surface temperatures, measured through a typical 24h period during the experiments.

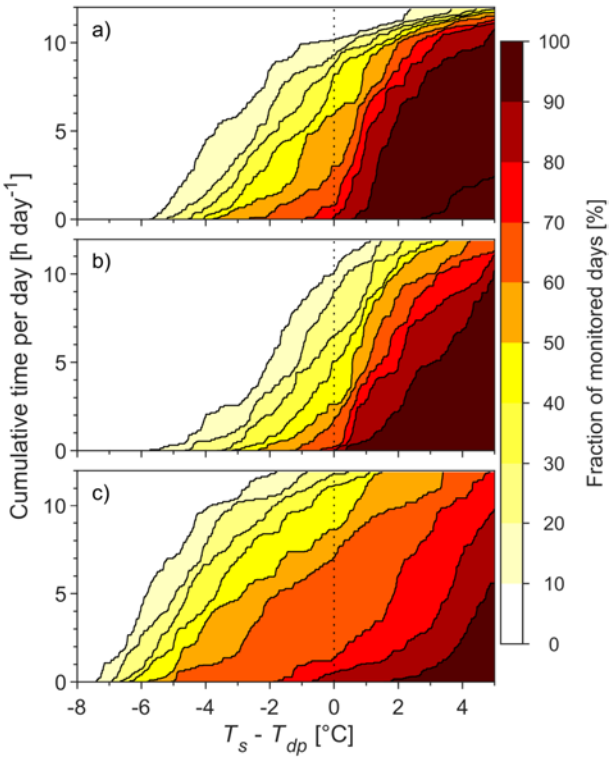

Figure 2: Time in which the mean roof surface temperature, T_s, was below the local dew point temperature, T_{dp}, during experiments at a) Nowra, b) Shellharbour, and c) Wetherill Park.

Roof condensation model

This section of the report describes the development and verification of a model that can simulate the water condensation/evaporation process on a roof surface. Several numerical case studies have also been presented, to demonstrate the influence of key variables under quasi-steady conditions.

Model development

Energy balance

The energy balance of a flat roof sheet is illustrated in Figure 3. Accordingly, the governing equation for the energy balance of a roof can be expressed using Equation 1, given the assumptions listed below:

- Heat transfer to/from the roof sheet lower surface is via conduction only (e.g. through a layer of insulation);
- The sensible heat capacitance of dew formed on the roof surface is negligible;
- The roof sheet and any accumulated dew are isothermal; and
- The roof surface radiative transmittance is zero (i.e. it is opaque).

$$c_{p,s} m_s \frac{dT_s}{dt} = \alpha_s G_t - q''_{conv} - q''_{lat} - q''_{rad} - q''_{cond} \quad (1)$$

Here, $c_{p,s}$ is the specific heat capacity of the roof material, m_s is the roof sheet mass per unit area, T_s is the roof surface temperature, t is time, α_s is the roof surface solar absorbtance, G_t is the solar heat flux incident on the roof surface, and q'' is a heat flux from the roof sheet; subscripts 'conv', 'lat', 'rad' and 'cond' signify convective, latent, radiative and conductive heat transfers, respectively. Equation 1 can be discretised, which allows the roof surface temperature to be calculated through a series of discrete time steps.

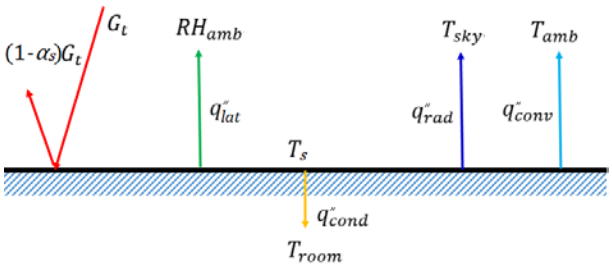

Figure 3: Energy balance of a flat roof.

External convective heat transfer

The convective heat flux from the external surface of the roof can be calculated using the expression:

$$q''_{conv} = \bar{h}_{conv}(T_s - T_{amb}) \quad (2)$$

where the $\bar{h}_{conv}$ is the spatially averaged convective heat transfer coefficient. Five of the most suitable models for $\bar{h}_{conv}$ have been compared in Figure 4, including the: i) ClearRoof model (Clear *et al.*, 2003), ii) model developed by Krisher and Kust (Holck and Svendsen, 2004), iii) TARP model (Walton, 1981), iv) DOE-2 model (LBL, 1994), and v) model developed by Mitchell (1976). Detailed descriptions of these models can be found in the corresponding references, so they have not been included here. The parameters used in the model comparison are summarised in Table 1; they represent two large (70,000m^2) roofs, with different length-to-width aspect ratios. The ASHRAE roughness factor and terrain roughness category were required by some of the models; values representing a relatively smooth roof surface within an urban terrain have been adopted here. For more details regarding these parameters, the interested reader is directed to ASHRAE (2009) and (Walton, 1981).

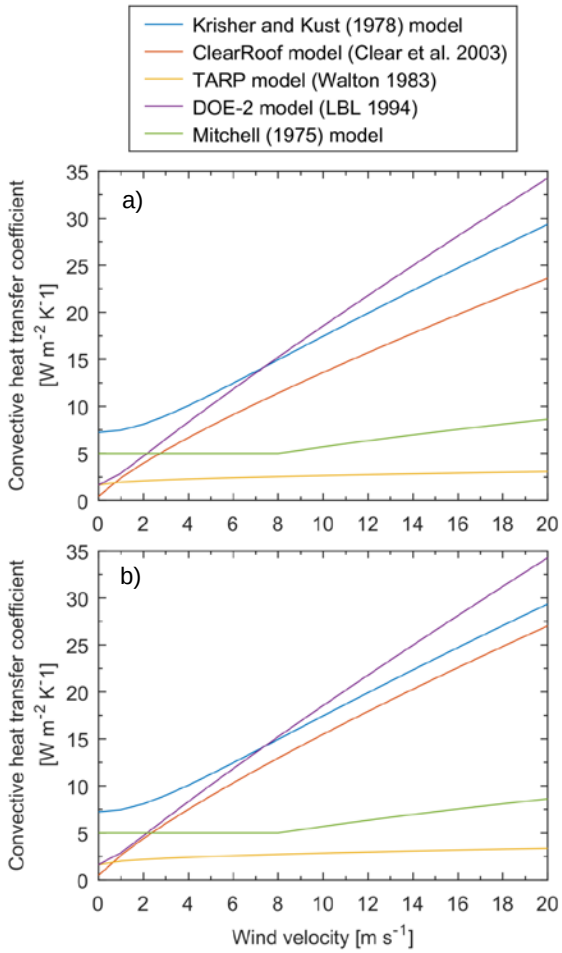

Figure 4: Comparison of external convective heat transfer coefficients calculated using different models, for a) Roof A, and b) Roof B.

Table 1: Summary of parameters used for the comparison of the external heat transfer coefficients calculated using different models.

Parameter	Roof A	Roof B
Roof surface temperature (T_s) [°C]	10	10
Ambient air temperature (T_{amb}) [°C]	20	20
Roof length (L) [m]	350	700
Roof width (W) [m]	200	100
Height above ground (H) [m]	10	10
Reference wind speed (u_{ref}) [m s^{-1}]	0–20	0–20
Wind direction relative to the normal of the roof length (θ) [°]	0	0
ASHRAE roughness factor (R_f)	1	1

The ClearRoof model, Krisher and Kust model, and DOE-2 model produced results that were fairly similar in the cases investigated; the TARP model and Mitchell model gave much lower $\bar{h}_{conv}$ values for wind speeds greater than 5 m s^{-1}. The obvious deviations indicated the importance to select an appropriate model to calculate the convective heat transfer coefficient. Previous studies have validated the ClearRoof model (Costanzo et al. 2014) and concluded that it was relatively accurate for near-horizontal roofs. The ClearRoof model is also takes into account many of the physical parameters that are important in the convective heat transfer process, e.g. roof surface roughness, roof size and wind direction. For these reasons, the ClearRoof model was adopted to determine $\bar{h}_{conv}$ in the roof condensation model developed here.

Latent heat transfer

The rate of latent heat released during condensation, and absorbed during evaporation, can be calculated as follows (Holck and Svendsen, 2004):

$$q''_{lat} = \dot{m}_{evap}\gamma = h_m \rho_{air} \frac{M_{water}\gamma}{M_{air}P_0}\left(P_{ws}|_{T_s} - P_{ws}|_{T_{dp}}\right) \quad (3)$$

where $\dot{m}_{evap}$ is the mass transfer rate per unit area, γ is the latent heat of vaporisation of water, h_m is the convective mass transfer coefficient, ρ_{air} is the density of air, M_{water} and M_{air} are the molecular weights of water and air, respectively, P_0 is the total barometric pressure, P_{ws} is the water vapour saturation pressure, and T_{dp} is the dew-point temperature. In the present work, $\dot{m}_{evap}$ is defined as positive for evaporation and negative for condensation.

Mass transfer of water to/from a surface via condensation/evaporation is similar to convective heat transfer, in terms of the limiting convection and diffusion processes that are involved. It has been shown that h_m is approximately proportional to $\bar{h}_{conv}$ and that one coefficient can be calculated from the other using the Lewis number, Le (Bergman *et al.*, 2011):

$$h_m = \frac{\bar{h}_{conv}}{\rho_{air} c_{p,air} Le^{1-n}} \quad (4)$$

Here, $c_{p,air}$ is the specific heat capacity of air. Bergman *et al.* (2011) demonstrated that it is assumed n = 1/3 for most applications.

If it is assumed that the physical properties of air and water are approximately constant in the range of temperatures that are of interest, substitution of appropriate values for γ, M_{water}, M_{air}, $c_{p,air}$, P_0 and Le into Equations 3, and combination with Equation 4, yields (Holck and Svendsen, 2004):

$$q''_{lat} \approx \begin{cases} 0.017\bar{h}_{conv}\left(P_{ws}|_{T_s} - P_{ws}|_{T_{dp}}\right) & T_s \geq 0 \\ 0.019\bar{h}_{conv}\left(P_{ws}|_{T_s} - P_{ws}|_{T_{dp}}\right) & T_s < 0 \end{cases} \quad (5)$$

External long-wave radiative heat transfer

The long-wave radiative heat transfer between the roof and the sky can be calculated using the expression:

$$q''_{rad} = \varepsilon_{eq}\sigma\left(T_s^4 - T_{sky}^4\right) \quad (6)$$

where T_{sky} is the sky radiative temperature, σ is the Steffan Boltzmann constant, and ε_{eq} is the apparent roof surface emissivity. T_{sky} can be estimated for clear (i.e. non-cloudy) conditions, at altitudes close to sea-level, as (Martin and Berdahl, 1984):

$$T_{sky} \approx T_{amb}\left(0.771 + 0.0056T_{dp} + 0.000073T_{dp}^2 + 0.013\cos\left(\frac{2\pi}{24}t_h\right)\right)^{0.25} \quad (7)$$

where t_h is the hour of day (starting at 0, at midnight). T_s, T_{sky} and T_{amb} must be expressed in Kelvin in Equations 6–7, and T_{dp} must be expressed in degrees Celsius.

If it is assumed that condensed water on the roof surface forms a film of uniform thickness, the apparent roof surface emissivity, ε_{eq}, depends on the dry roof emittance, ε_s, and the water film thickness, δ. The dew film thickness expressed in μm is equivalent to the average dew mass load, expressed in g m^{-2}. In the roof condensation model developed here, ε_{eq} is estimated using the following expression (Xu and Shen, 1992):

$$\varepsilon_{eq} = \begin{cases} \varepsilon_s, & \text{for dry roof} \\ \frac{(1-\rho_{water})[1-\rho_s exp(-2\alpha_A\delta)]}{1-\rho_s\rho_{water}exp(-2\alpha_A\delta)}, & \text{for wet roof} \end{cases} \quad (8)$$

Here, α_A is twice the Lambert absorption coefficient, ρ_{water} is the reflectance for long-wave radiation arriving from the water side, and ρ_s is the reflectance of the roof-water interface, which is equal to $(1 - \varepsilon_s)$. The value used for α_A in the present study was 0.1184, which approximately equals the mean value averaged over an infrared range from 8×10^2 nm to 3×10^5 nm (ZOLOTAREV and VM, 1969; Hale and Querry, 1973; Downing and Williams, 1975). The value of ρ_{water} was set as 0.04, which is the hemispherical average infrared value integrated from data reported by Sidran (1981).

In order to assess the validity of the apparent emissivity model in Equation 8, experimental data from Bassett and Trethowen (1984) was compared to the model (see Figure 5). The modelled and measured values agreed very well in this case, involving a low-emissivity foil

surface, with a root mean square error (RMSE) of 0.0354.

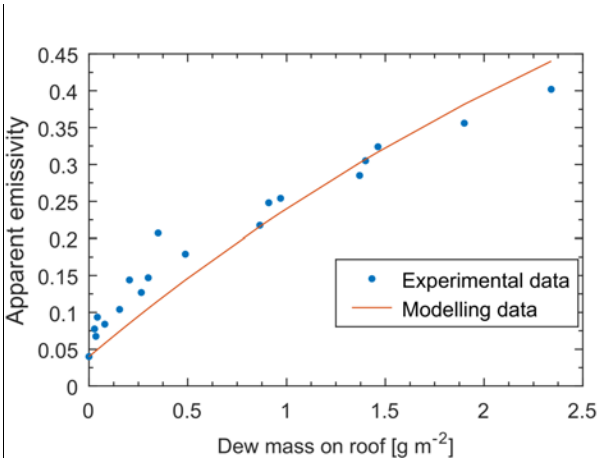

Figure 5: Comparison of the apparent emissivity model with experimental data.

The effect of a water film on the effective thermal emittance of three typical roofing materials is illustrated in Figure 6. It can be seen that a dramatic change can occur with small changes in the dew condensation, when it is lower than 10 g m^{-2} (i.e. when dew water film thickness $\delta \lesssim 10$ μm). For thicker water films, the effective surface emittance approaches the emissivity of a limit for bulk water, which appears to have been effectively reached for dew mass loadings above 20 g m^{-2} (i.e. dew water film thickness $\delta \gtrsim 20$ μm).

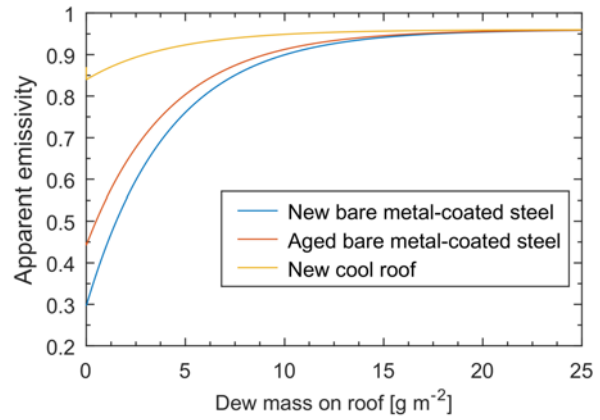

Figure 6: Effect of a water film on the apparent thermal emittance of roof surfaces.

External short-wave radiative heat transfer

Short-wave (i.e. solar) radiative heat transfer has not been included in the roof condensation model for two reasons: i) roof condensation predominantly occurs at night, when there is no significant short-wave radiative transfer, and ii) water films have been shown to have a relatively small effect (~2-3% for solar radiation from normal direction) on the effective short-wave absorbtance of surfaces.

Conductive heat transfer below roof

Heat transfer from the roof sheet to the indoor environment can be approximated as:

$$q''_{cond} = U(T_s - T_i) \quad (9)$$

where T_i is the indoor air temperature, and U is the overall thermal conductance between the roof sheet and the indoor environment. U can be calculated from the internal convective heat transfer coefficient, h_i, and the thermal resistance of the roof structure below the roof sheet, R_s:

$$U = 1/(R_s + 1/h_i) \quad (10)$$

In this simplified approach, radiative heat transfer within the building is neglected. This simplification should not have a large effect on results for well-insulated roofs, and when the model is implemented in BPS, the simulation software will account for radiation within the building.

Model integration

By combining Equations 1, 2, 5, 6, 7, 8, 9 and 10 with the ClearRoof model, and establishing a set of boundary conditions (including T_{amb}, RH_{amb}, T_i, G_t, α_s, ε_s, m_s, $c_{p,s}$, t_h, the roof dimensions, roof surface roughness, reference wind speed (u_{ref}) and wind direction(θ)), changes in the water condensation rate and the roof surface temperature over time can be estimated. In the present work, the Euler method was used to solve the discretised differential equations.

Quasi-steady case studies

To investigate fundamental aspects of the condensation/evaporation process of dew on a roof with relatively high dry thermal emittance (0.85), several quasi-steady cases were simulated using the roof condensation model. Three simulations were run with the steady boundary conditions summarised in Table 2. In one the effects of dew on the roof energy balance were not included at all, in the second only the effects of dew on apparent emissivity were included, and in the third both emissivity and latent heat effects were included. Simulations were then run with a range of ambient air temperatures and humidities (ranging from 12°C to 22°C and 70% to 90%, respectively), to investigate the effect of these parameters on dew condensation process.

Table 2: Steady boundary conditions used in the modelling.

Parameter	Value
Initial roof surface temperature ($T_{s,initial}$) [°C]	10
Ambient air temperature (T_{amb}) [°C]	15
Ambient relative humidity (RH_{amb}) [%]	80
Effective sky radiative temperature (T_{sky}) [°C]	-1.73
Indoor air temperature (T_i) [°C]	20
Roof length (L) [m]	350
Roof width (W) [m]	200
Height above ground (H) [m]	10
Reference wind speed (u_{ref}) [m s^{-1}]	10
Wind direction relative to normal of the roof length (θ) [°]	0
ASHRAE roughness factor (R_f)	1
Terrain roughness category	4
Dry-roof emissivity (ε_s)	0.85
Overall thermal conductance between the roof sheet and the indoor environment (U) [W m^{-2} K^{-1}]	0.5
Roof mass per unit area (m_s) [kg m^{-2}]	3.959
Specific heat capacity of the roof ($c_{p,s}$) [kJ kg^{-1} K^{-1}]	0.5
Barometric pressure (P_0) [kPa]	101.325
Time of day (t_h) [h]	0
Latent heat of vaporisation (γ) [kJ kg^{-1}]	2501

Effects of condensation

Figure 7 presents results from the thermal balance process. It can be seen from Figure 7a that the roof temperature increased rapidly in this case, before decreasing gradually towards a limit, where thermal equilibrium was reached. The dew condensation rate also approached a limit; however, the limit was greater than zero, so the water film thickness was steadily increasing with time.

The two primary mechanisms by which roof condensation can affect roof temperatures are explored in Figure 7b. The overall effect of roof condensation on the quasi-steady roof temperature was only 0.03°C. However, rapid condensation in the early phase of the simulation did produce a temporary difference in roof temperature of up to 0.49°C, as compared to the case in which condensation effects were not included. When only the effect of condensed water on the apparent roof emissivity was included (i.e. when the release and absorption of latent heat were ignored), a quasi-steady roof temperature was reached that was 0.3°C lower than that reached without any condensation effects. Under the steady boundary conditions investigated in this case, it seemed that the effects of the roof condensation on the apparent roof emissivity and the release/absorption of latent heat cancelled each other out to some extent; however, both effects seemed to be significant. Given other steady boundary conditions or dynamic boundary conditions, the two effects could combine to affect roof temperatures significantly.

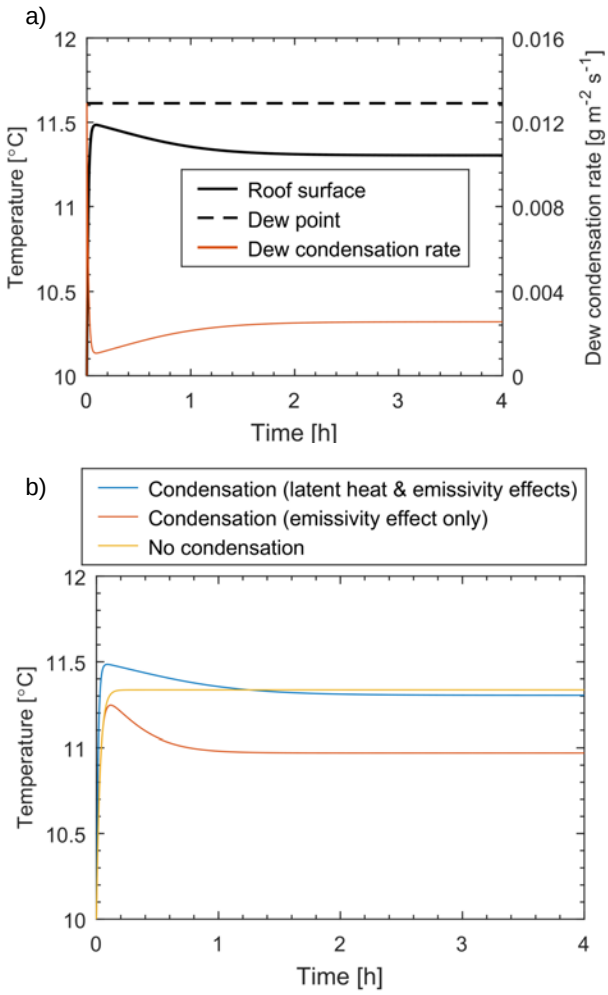

Figure 7: Development of a quasi-steady roof surface temperature, as predicted by the model: a) plotted with dew point temperature and the condensation rate, and b) compared with results obtained without taking latent heat effects and/or emissivity effects into account.

Influence of ambient humidity

Figure 8 presents the quasi-steady roof temperature reached after 4 simulated hours, given various levels of ambient humidity. It can be seen from Figure 8a that higher roof temperatures tended to be reached when the ambient humidity was increased. In cases where a roof surface temperature less than the dew-point temperature was reached, condensation continued to occur in the quasi-steady state, which increased the roof surface temperature.

Figure 8b compares the quasi-steady roof temperatures from Figure 8a with those obtained without any roof condensation effects, and with the condensation effects on roof emissivity only (i.e. neglecting the release and absorption of latent heat). It is evident that it is the latent heat release during condensation that has affected the

slope of the roof temperature plot in Figure 8a. The effect of a water film on the roof thermal emittance also had a significant effect on quasi-steady roof surface temperatures, but it seemed that the magnitude of that effect did not depend on the ambient humidity. It is also evident in Figure 8 that water condensation can have a significant effect on roof temperatures in some conditions (around 0.83°C in the cases studied here).

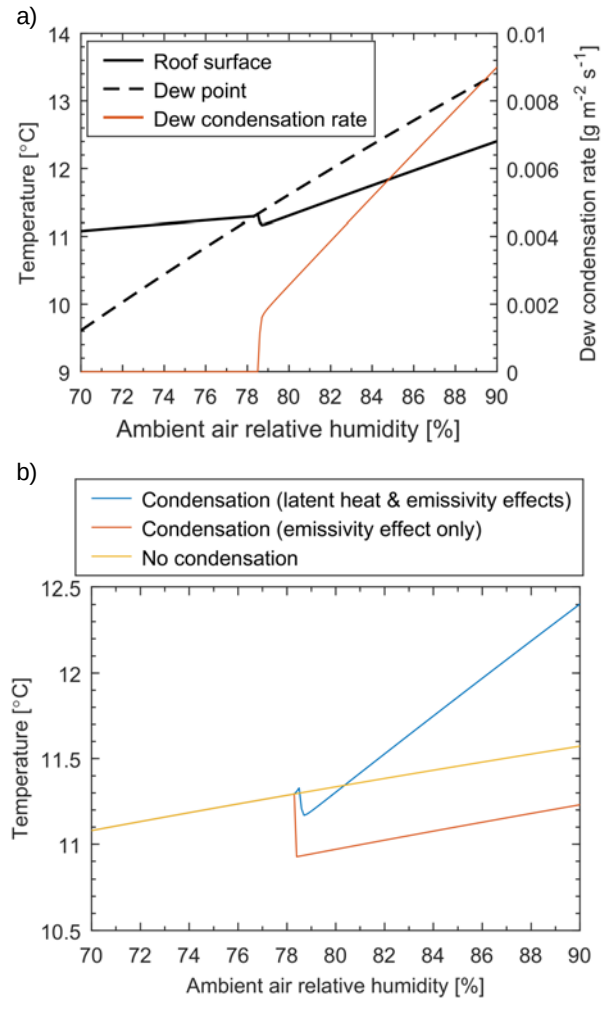

Figure 8: Effect of ambient humidity on the quasi-steady conditions reached after 4 simulated hours: a) temperatures and the condensation rate, and b) temperatures, given different condensation effects.

Influence of ambient air temperature

Figure 9 presents the effect of the ambient air temperature on the quasi-steady roof temperature and condensation rate (see Figure 9a) and heat fluxes (see Figure 9b) that were reached after 4 simulated hours. The magnitude of the condensation rate was driven by the difference between the roof surface temperature and dew-point temperature; for ambient air temperatures above 20°C, the roof surface temperature rose above dew-point, so the condensation rate went to zero. Latent heat fluxes were significantly smaller than convective and radiative heat fluxes in the cases investigated. If the dry-roof emittance had been significantly lower than the bulk-water emittance (e.g. if it had been a metal-coated steel roof), it could be expected that the effects of condensation on the radiative heat flux would be much larger than the latent heat effects in these cases. The extension of this work to transient boundary conditions in BPS, as discussed later in this report, revealed such details more clearly.

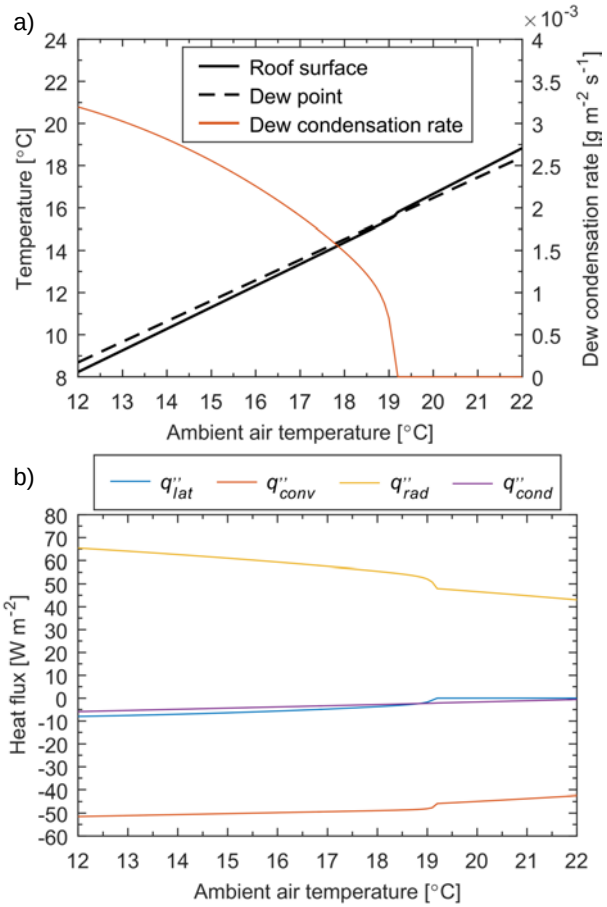

Figure 9: Effect of ambient air temperature on the quasi-steady conditions reached after 4 simulated hours: a) temperatures and the condensation rate, and b) latent (q''_{lat}), convective (q''_{conv}), radiant (q''_{rad}), and conductive (q''_{cond}) heat fluxes.

Equivalent case studies for a low-emissivity roof

The same quasi-steady case studies were undertaken for a bare metal-coated steel roof, under the same simulated conditions as the painted roof. In order to keep this section of the report relatively brief, these additional results have been included in an Appendix.

Experiments into dew runoff

The roof condensation model developed in the previous section of this report did not take water runoff into account. Therefore, the model could potentially predict unrealistically large quantities of accumulated dew, and therefore overestimate the duration of evaporation. To address this issue, a set of experiments were conducted to determine an approximate upper limit to the quantity of dew that could accumulate on low-angled metal sheet roofs. This limit was then included in the roof condensation model, to reduce the risk of over-prediction of dew mass loads.

Experimental method

A 540 × 235 mm^2 sample of 'Lysaght Kliplok High Strength' steel sheet was fitted to an enclosure made of 100 mm-thick expanded polystyrene, such that the steel sheet formed the top of the enclosure (see Figures 10 and 11). A plastic container filled with ice was placed in the enclosure, almost filling the space under the steel sheet, and the entire enclosure was placed on an AND EK-6100i precision balance within a climate-controlled chamber. Thus, the steel sheet was cooled by the ice underneath, and the temperature and humidity of the air above could be controlled to induce condensation on the top surface of the sheet. The balance was used to track the mass of accumulated condensate over time, recording measurements every 10 s.

Figure 10: Steel roof sheet sample fitted to the polystyrene enclosure, within the climate chamber.

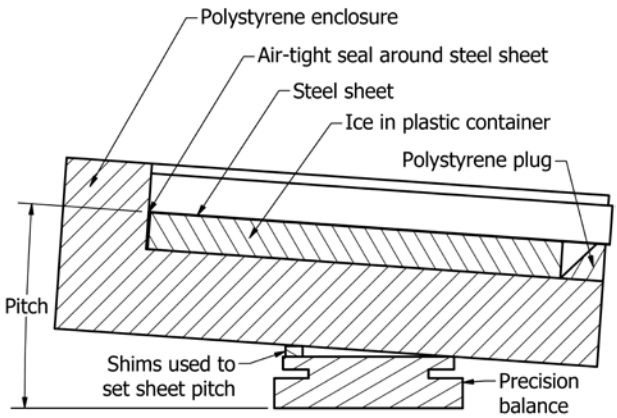

Figure 11: Cross-section of the experimental setup.

Experiments were conducted with the sheet inclined at various angles from the horizontal, corresponding to roof pitches of 1, 2, 4 and 8°. The air inside the chamber was maintained at 20°C and 95% RH during all experiments, except for three additional experiments conducted with a 2° pitch at 40°C and 95% RH, to investigate the sensitivity of the runoff process to the condensate temperature.

Each experiment was continued until a pseudo-steady condensate mass load was established, i.e. until the time-averaged rates of water runoff and condensation were in approximate equilibrium. This typically resulted in experiments lasting 10–14 h. The steel sheet and condensate temperature was measured during several of the experiments, using an infrared thermometer.

Despite the relatively low thermal conductance of the polystyrene enclosure, and the air-tight seal formed around the edges of the steel sheet, a small amount of condensate did form on (and possibly inside) the polystyrene enclosure, in addition to that on the steel top surface. It was necessary to correct the mass measurements for this extraneous condensation. At the end of each experiment, water was removed from the steel sheet top surface and the enclosure final mass was recorded. The difference between the enclosure initial (dry) mass and the final mass (with the steel sheet wiped dry) was a measure of extraneous condensate that had accumulated during the test. By assuming that this condensate formed at a steady rate, its mass could be estimated for each point in time through an experiment and subtracted from the corresponding mass measurements that had been recorded.

Results and discussion

The steel sheet temperature was not uniform in space or time during the experiments. When the surrounding air was controlled to 20°C and 40°C, the steel sheet was measured to be 15 ± 4°C and 34 ± 4°C, respectively.

Condensation was observed to form on the steel sheet almost immediately. Initially, microscopic droplets gave the surface a dull grey appearance, but they coalesced to form visible droplets at a relatively low condensate mass load of approximately 25 g m^{-2}. These droplets continued to intermittently coalesce to form larger drops.

The first flow of droplets across the sheet was observed on the steep surfaces formed by the steel corrugations, at a condensate mass load of approximately 130 g m^{-2}, as the gravitational forces pulling individual droplets down the slope overcame the surface tension forces retaining them in place. These droplets stopped flowing as they reached the base of the corrugation, and microscopic droplets of condensate started to form on the trail of dry steel left behind (see Figure 12a). At a condensate mass load of 190–290 g m^{-2}, enough water accumulated at the base of the corrugations to break the holding surface tension forces and flow down and off the end of the steel sheet. Intermittent runoff events of this type (initiating at the base of the corrugations) continued to occur, while droplets on the relatively flat pan section of the sheet continued to coalesce until they were large enough to initiate runoff flow as well. Eventually, a

pseudo-steady condensate load was reached, as intermittent localised runoff events reached a time-averaged equilibrium with the steady condensation occurring over the entire steel surface (see Figure 12b).

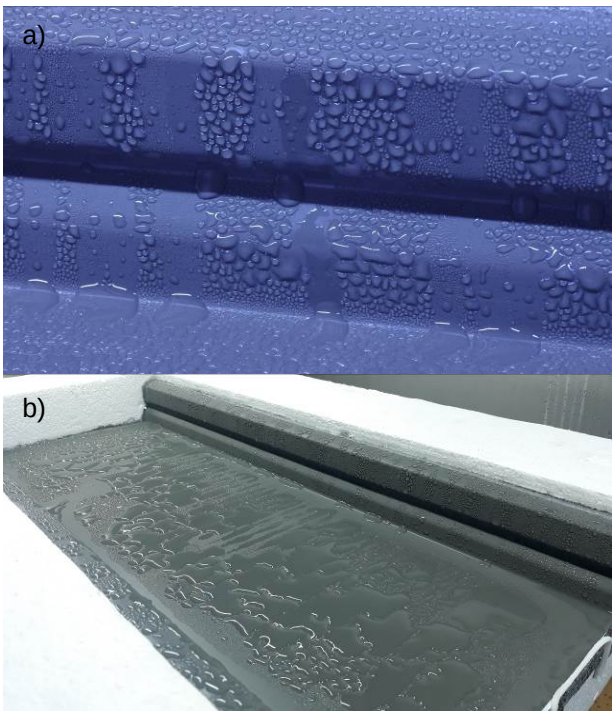

Figure 12: Condensate on the steel sheet, showing: a) the steep surface formed by the steel corrugation, and b) a pseudo-steady condensate mass load. Small droplets, forming in paths of recent runoff events are visible in both images.

Three primary phases could be identified in the condensation process (see Figure 13): i) initially, condensation formed at a relatively steady rate; ii) after the first flow of water off the end of the steel sheet, the condensate load continued to increase but at a reduced effective rate due to intermittent runoff events; and iii) eventually a pseudo-steady condensate load was reached.

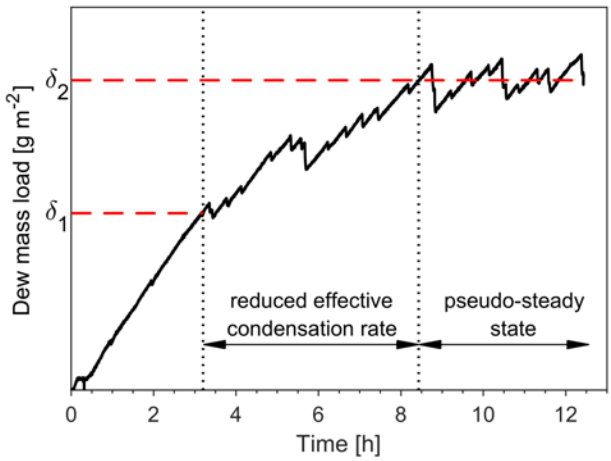

Figure 13: Example of the condensate accumulation recorded through one experiment.

Two condensate mass loads, δ_1 and δ_2, were defined as those at which runoff from the sheet began and at which the pseudo-steady state was reached, respectively. δ_2 was calculated as the first condensate mass load from the measured time-series that exceeded the average of all subsequent measurements. A condensation reduction factor, λ, was also defined, to characterise the effect of intermittent runoff events in the second phase of the condensation process:

$$\lambda = \left(\frac{\delta_2 - \delta_1}{t_2 - t_1}\right) C^{-1} \quad (11)$$

Here, t_1 and t_2 are the times at which condensate mass loads of δ_1 and δ_2 were first reached, respectively, and C is the mean condensation rate recorded between t_1 and t_2, not including times at which the condensate mass load was decreasing due to runoff. Thus, λ represents the ratio of the effective condensation rate (taking into account both condensation and runoff) to the condensation rate that occurs between runoff events.

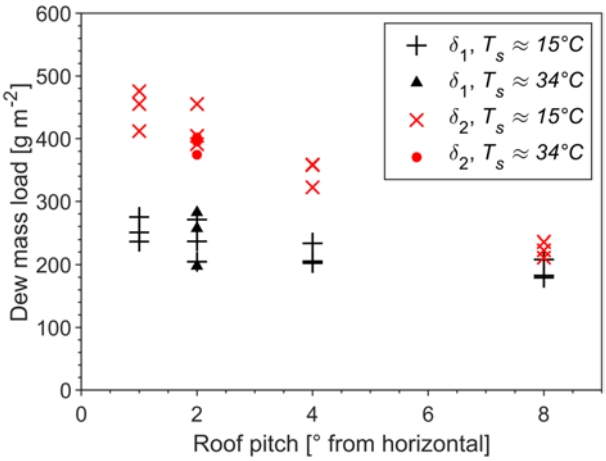

Figure 14: Influence of roof pitch on the dew mass loads at which runoff begins (δ_1) and at which a pseudo-steady upper limit is reached (δ_2). Results obtained with a higher sheet surface temperature ($T_s \approx 34°C$) and roof pitch of 2° have also been plotted, for comparison.

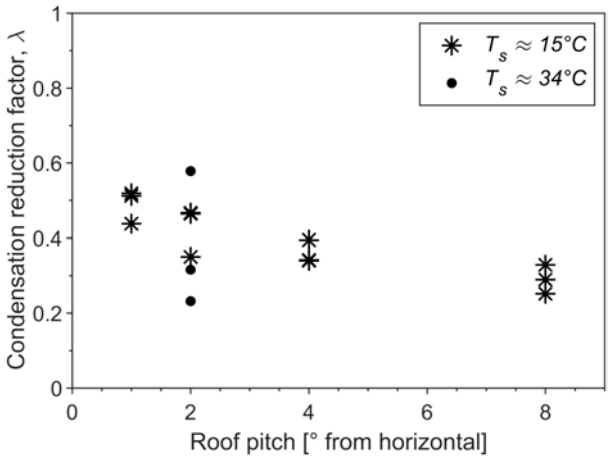

Figure 15: Influence of roof pitch on the condensation reduction factor, λ. Results obtained with a higher sheet surface temperature ($T_s \approx 34°C$) and roof pitch of 2° have also been plotted, for comparison.

The influence of roof pitch on δ_1, δ_2 and λ are presented in Figures 14 and 15. Within the range of pitches investigated, decreases in roof slope caused an increase in all three parameters; the mean values of δ_1, δ_2 at each roof pitch varied from 190 to 254 g m^{-2} and from 223 to 448 g m^{-2}, respectively, and the mean values of λ varied from 0.29 to 0.49.

Results from the three tests conducted at higher temperatures did not vary significantly from those obtained with the same roof pitch (2°) and lower temperatures. For an increase in temperature from 15 to 34°C, the kinematic viscosity and surface tension of pure water decreases by 35% and 4.0%, respectively (Vargaftik *et al.*, 1983; Gebhart *et al.*, 1988). For condensate droplets on an inclined surface, such changes in fluid properties would reduce the droplet mass at which surface tension forces are overcome, and the nature of runoff flow once it has begun. Changes in surface energy brought about by temperature change could also change the wetting characteristics of condensate on the roof surface, thereby influencing runoff. However, these effects were not large enough to be clearly resolved in the results presented here, given the experimental repeatability that was attained.

It is important to note that the results presented here were obtained with a new, clean painted steel sheet, with only one corrugation profile (consisting of one wide flat pan between corrugations). It is likely that dew runoff from roofs with different geometric profiles or surface properties (e.g. from surface ageing and soiling) is significantly different from that characterised here. Furthermore, the relatively short length of the roof sample used in the experiments (540 mm) could have influenced the results significantly. On real roofs, it is possible that droplets flowing from higher on the roof keep dew mass loads lower than the upper-limits measured here. Further investigation into this issue would be valuable. Since no other data of this type was found in the literature, the experiments reported here offer a useful starting point for simple models of dew runoff from roofs. However, the limitations of the data should be understood by users of such models.

Implementation in the roof condensation model

In order to include the effects of water runoff in the roof condensation model, the change in the dew mass load during one timestep (from δ^k to δ^{k+1}) was calculated as follows:

$$\delta^{k+1} = \begin{cases} \delta^k - \frac{1000\Delta t q''_{lat}}{\gamma} & q''_{lat} \geq 0 \\ \delta^k - \frac{1000\Delta t q''_{lat}}{\gamma} & q''_{lat} < 0, \quad \delta^k \leq \delta_1 \\ \delta^k - \lambda\frac{1000\Delta t q''_{lat}}{\gamma} & q''_{lat} < 0, \quad \delta_1 < \delta^k \leq \delta_2 \\ \delta^k & q''_{lat} < 0, \quad \delta_2 < \delta^k \end{cases} \quad (12)$$

Here, Δt is the timestep duration [s], q''_{lat} is the latent heat flux calculated for the timestep [W m^{-2}], γ is the latent heat of vaporisation of water [J kg^{-1}], and the dew mass values δ^k, δ^{k+1}, δ_1 and δ_2 are expressed in units g m^{-2}. Thus, simulated evaporation rates are not modified, and simulated condensation rates are either unmodified, reduced or neglected, depending on the amount of dew on the roof. Heat fluxes were not modified or introduced to account for runoff, since it was assumed that any water flowing from the roof surface was at the surface temperature.

Above-roof temperature model

The air temperature field above a roof surface is the product of surrounding air temperatures, the roof surface temperature, and air flow, which can be driven by inertial (i.e. wind) and buoyant (i.e. thermal) forces. Heat will diffuse between the roof surface and air in contact with that surface. The vertical transport of heat, via diffusion and convection, will then produce a distribution of air temperatures between the surface and a 'reference height', where the effect of the roof surface temperature is small enough for the local air temperature to be considered equal to the reference 'ambient' air temperature. It is desirable to be able to predict such vertical temperature profiles, so that realistic inlet air temperatures can be assigned to rooftop HVAC equipment in BPS.

The empirical above-roof temperature model developed in RP1037 predicts air temperatures near a roof surface, given four input variables: i) a reference wind speed, u_{ref}, ii) the mean roof surface temperature, T_s, iii) the 'ambient' air temperature, T_{amb}, and iv) a roof length scale, L (Green *et al.*, 2018). It is based on the premise that the vertical temperature profile above a roof surface will be approximately logarithmic, varying from the roof surface temperature at the roof surface to the 'ambient' air temperature at a reference height.

To the best of the authors' knowledge, the experimental dataset on which the model was based (and which was developed in RP1037) is much more comprehensive than those produced in previous investigations of above-roof air temperature fields (e.g. Leonard and Leonard (2006); Wray and Akbari (2008); Carter (2011); Pisello *et al.* (2013); Carter and Kosasih (2015)), in terms of the number of measurements that were taken, the set of meteorological parameters that were measured locally, and the number of experimental sites that were studied. However, the RP1037 experiments did include only three shopping centre buildings, and the relatively warm weather conditions that occurred near Sydney, Australia, during the period December 2017–May 2018. It is important that any limitations in the validity of the model, which may arise from the limited scope of this dataset, be well understood.

Applicability of the model to cold weather

Since the above-roof temperature model predicts the response of an air temperature field to a hot or cold roof surface, and wind, the parameters that define the range of weather conditions on which it has been based are: i) the difference between roof surface temperature and 'ambient' air temperature, $T_s - T_{\mathrm{amb}}$, and ii) the reference wind speed, u_{ref}. While many other parameters do affect near-roof air temperatures (e.g. the solar heat flux, roof insulation or degree of cloud cover), they do so indirectly, via the effect that they have on u_{ref} or $T_s - T_{\mathrm{amb}}$.

Figure 16 compares the range of $T_s - T_{\mathrm{amb}}$ and u_{ref} covered by the RP1037 experimental dataset with those simulated in the RP1037 BPS. The simulated T_{amb} and u_{ref} values came from reference meteorological year weather files for seven Australian cities, representing seven of the eight primary Australian climate zones defined in the Australian National Construction Code (Australian Building Codes Board, 2016), and the simulated T_s values were calculated during simulations of the shopping centre building model, developed in RP1037, in those climate zones (Green *et al.*, 2018). The parameter bounds presented for each climate zone in Figure 16 include the combined set of T_s values from simulations of the shopping centre with a new cool roof, a new metal-coated roof and an aged metal-coated roof, throughout the entire simulated year.

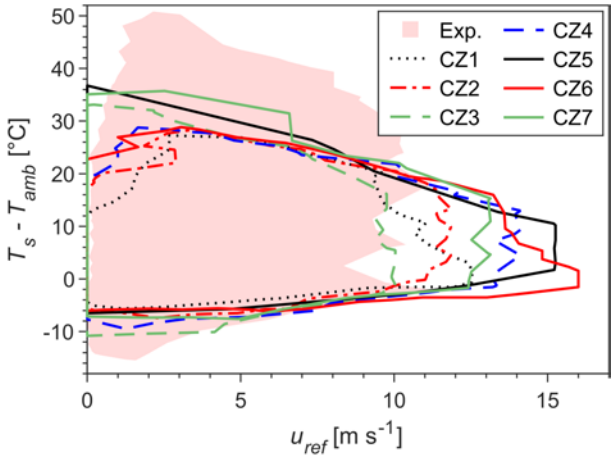

Figure 16: Comparison of the range of conditions that occurred during the experiments in RP1037 (labelled 'Exp.'), with those from year-long building performance simulations of a shopping centre in seven Australian climate zones (labelled 'CZ1'–'CZ7').

Even though the RP1037 experiments were undertaken in relatively warm conditions (near Sydney, in summer and autumn), the wide range of weather conditions included in the year-long simulations of seven climate zones (including many examples of cold winter weather) did not give rise to combinations of $T_s - T_{\mathrm{amb}}$ and u_{ref} that were far from those that occurred during the experiments, except for high wind speeds of $u_{ref} \gtrsim 10$ m s^{-1}. This result supports the validity of the above-roof temperature model in such simulations. The lack of high wind speeds in the experimental dataset indicates that the model can currently only provide near-roof air temperature predictions for such conditions with a relatively large degree of uncertainty. Further validation of the model in these (and indeed, all) conditions would be valuable. However, the effect of any model inaccuracy at high wind speeds on simulated annual HVAC energy consumption would be relatively small in the cases investigated here and in RP1037, since: i) wind speeds over 10 m s^{-1} were very uncommon in the simulations (see Figure 17); and ii) near-roof air temperatures tend to deviate less from the 'ambient' air temperature in strong winds, as the roof surface is brought closer to the 'ambient' temperature by enhanced convective heat transfer, so the model has a relatively small effect on HVAC performance in these conditions anyway.

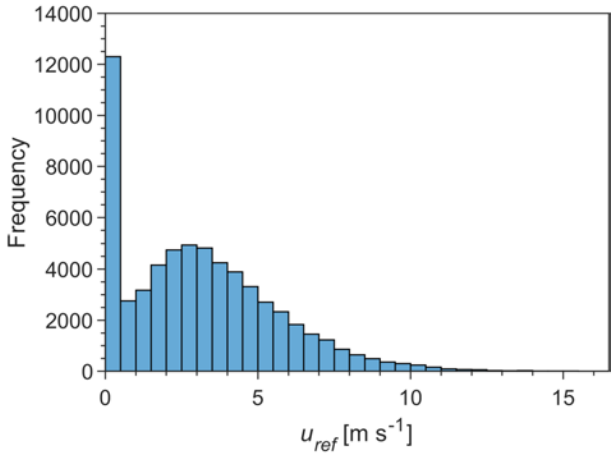

Figure 17: Histogram showing the occurrence of different wind speeds in reference meteorological year weather files for cities in climate zones 1–7.

Applicability of the model to other buildings

The RP1037 experimental dataset was collected from three case-study shopping centre buildings, so care should be taken when applying the above-roof temperature model to buildings or settings much different than those case-studies. Parameters that are likely to have a significant effect on air temperature fields above roofs include:

- Roof size;
- Roof aspect ratio;
- Roof slope;
- Building height; and
- Topography surrounding the building.

The three case-study buildings had roof areas in the range 15,000–77,000 m^2, with aspect ratios less than 3. Although the above-roof temperature model does account for roof size to some degree, it is currently not possible to determine whether it produces accurate results for buildings with roof areas far outside this range, or high aspect ratios. All three buildings had low-angle (<5° from horizontal) roofs, so the model may not accurately predict temperature profiles above roofs with a significantly higher slope. The case-study buildings were approximately 5–20 m tall and were not in close proximity to any taller buildings that could significantly alter incoming wind flow. Therefore, the above-roof temperature model may not be appropriate for use in simulations of tall buildings, or buildings located near large obstructions to air flow.

Experimental measurements of air temperatures above the roofs of more buildings, and the local meteorological conditions, would be highly valuable since they would allow these unknown aspects of the above-roof temperature model to be better understood. Until this has occurred, care should be taken in applying the empirical model to buildings much different from those described above.

Revision of the above-roof temperature model

While conducting the analysis of the RP1037 data described above, it was recognised that a superior fit to experimental data could be achieved by altering the mathematical form of the above-roof temperature model slightly. Thus, an improved above-roof temperature model has been developed and presented here.

The primary change that has been made is in the equation for the shape parameter, α, in unstable conditions (i.e. when $T_s > T_{amb}$). In the old model, α was a function of the Richardson number, Ri (see Equation 13), only, whereas in this new version of the model, α is allowed to vary with $T_s - T_{\mathrm{amb}}$ and u_{ref} independently. A planar surface was fitted to the unstable data, using a least-squares technique. This change reduced the RMS deviation between modelled and measured air temperatures in unstable conditions from 0.83°C to 0.56°C. The new model is described by Equations 13–16, and Figure 18 presents the fit of the new model to the RP1037 experimental data.

$$Ri = \frac{g\beta(T_s - T_{amb})L}{u_{ref}^2} \tag{13}$$

$$\alpha = \begin{cases} -8.983 + 0.03607u_{ref} - 0.2205(T_s - T_{amb}) & Ri \geq 0 \\ -13.08 & -10^{-0.51} \leq Ri < 0 \\ -9.025 + 4.055\sin\left(\frac{\pi}{2}(\log_{10}(-Ri) - 0.64)\right) & -10^{1.79} \leq Ri < -10^{-0.51} \\ -4.97 & Ri < -10^{1.79} \end{cases} \tag{14}$$

$$T_{HVAC} = \frac{1}{z_2 - z_1}\int_{z_1}^{z_2}\left(T_s - (T_s - T_{amb})\frac{\ln\left(\frac{z+10^{\alpha}}{10^{\alpha}}\right)}{\ln\left(\frac{8+10^{\alpha}}{10^{\alpha}}\right)}\right)dz \tag{15}$$

$$T_{HVAC} = T_s - \frac{(T_s - T_{amb})}{(z_2 - z_1)\ln\left(\frac{8+10^{\alpha}}{10^{\alpha}}\right)}\left[(z_2 + 10^{\alpha})\ln\left(\frac{z_2+10^{\alpha}}{10^{\alpha}}\right) - z_2 + z_1 - (z_1 + 10^{\alpha})\ln\left(\frac{z_1+10^{\alpha}}{10^{\alpha}}\right)\right] \tag{16}$$

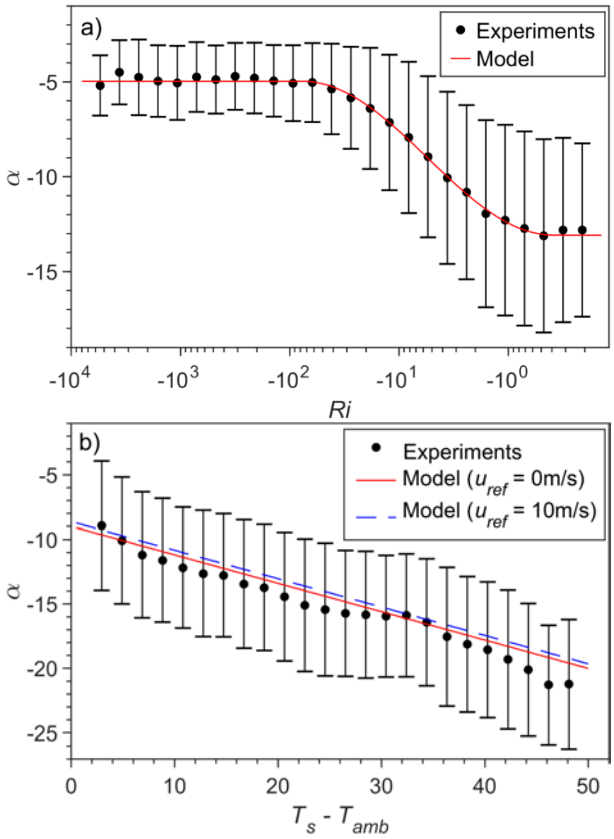

Figure 18: Comparison of the thermal boundary layer shape parameter, α, obtained from experimental data with those predicted by the above-roof temperature model, in a) stable and b) unstable conditions. Experimental data has been represented by the mean (dot) and standard deviation (whiskers) of α within discrete bins.

Building performance simulations

A parametric BPS study was conducted, incorporating the roof condensation model and the revised above-roof temperature model. A similar set of cases were investigated as had been in the previous project, RP1037. The primary differences between this and the previous investigations were the inclusion of the roof condensation model, adoption of the revised above-roof temperature model, and revision of several HVAC sizing and control settings to form a more realistic representation of the large-footprint buildings of interest. Therefore, the results presented here should be considered to supersede those contained in the RP1037 final report (Green *et al.*, 2018).

Aims

The parametric study was conducted with three primary aims:

1. Quantify the influence of cool roofs on the annual energy demand of large-footprint buildings in Australian climates, taking into account:
   a) the effect of water condensation and evaporation on the roof external surface; and
   b) the effect of the near-roof air temperature field on rooftop HVAC equipment.
2. Quantify the difference between BPS results that do and do not take these phenomena into account.

In order to achieve the aims outlined above, simulations were run of a case-study large-footprint building operating in a variety of Australian climates over the period of one year. The simulations were replicated with different cool roofs and a 'non-cool' bare metal-coated steel roof, and different types of HVAC equipment. In order to quantify the effects of near-roof air temperature fields and dew, each simulation was run with both the above-roof temperature and roof condensation models, with each model individually, and with neither model.

Simulation methodology

The BPS software EnergyPlus v8.9 was used, with the simulation manager jEPlus v.1.7.2 (Zhang, 2011). The Energy Management System (EMS) feature in EnergyPlus provides a means to manipulate simulation variables using custom scripts, thereby allowing the effective integration of external models.

Implementation of the above-roof temperature model

The revised above-roof temperature model was implemented using the EMS. At each timestep in the simulations, the ambient air temperature (T_{amb}) and reference wind speed (u_{ref}) were obtained from the weather file, the representative building length scale (L) was set as the square root of the total building roof area, and the mean roof surface temperature (T_s) was obtained from the current building energy balance. Using this information, a corrected inlet air temperature (T_{HVAC}) was determined for rooftop HVAC equipment, assuming that the equipment inlets span from $z_1 = 0.5$ m to $z_2 = 2$ m above the roof surface. Figure 19 depicts this process schematically.

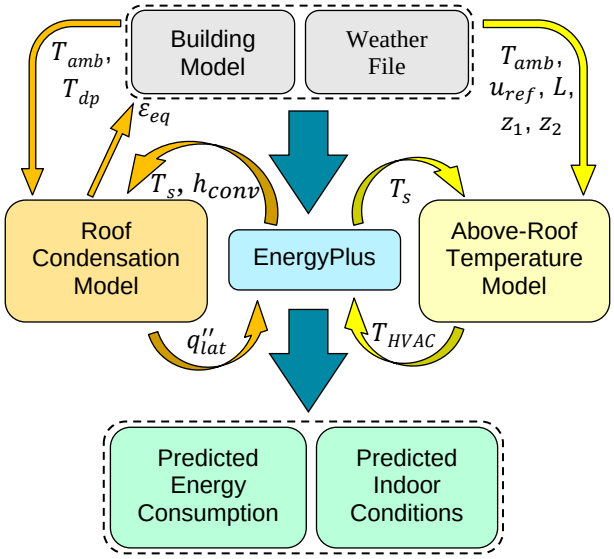

Figure 19: Schematic showing how the roof condensation and above-roof temperature models were integrated with EnergyPlus.

Implementation of the roof condensation model

The roof condensation model was implemented in EnergyPlus using the EMS, as shown in Figure 19. At each timestep within simulations, the current ambient temperature (T_{amb}) and dew-point temperature (T_{dp}) were obtained from the weather file, and the spatially averaged roof surface temperature (T_s) and roof convective heat transfer coefficient ($\bar{h}_{conv}$) were obtained from the previous timestep solution. These inputs were used to calculate: i) the latent heat released/absorbed due to condensation/evaporation of dew on the roof surface (q''_{lat}), and ii) the apparent roof thermal emittance taking into account the effect of any dew on the surface (ε_{eq}). A heat source term in the roof energy balance and the roof material thermal emittance could then be set to account for the effects of dew during the current timestep.

There was a risk that implementation of the roof condensation model in this way could cause instability in the simulations or incorrect results, since it uses an explicit method (i.e. uses variables from one timestep to estimate conditions at a future timestep). Therefore, it was important that an appropriately small timestep be used, to produce results that were timestep-independent and free of significant timestep-induced oscillations. A timestep sensitivity study was conducted to select an appropriate timestep for the proceeding simulations.

It was also important to check whether the thermal capacitance of dew on the roof could have a significant effect on the building performance, since the model implementation described above does not take such effects into account. Simulations were conducted in which the thermal capacitance of the roof sheet was

modified at each timestep according to the amount of dew present, and the results were compared to those obtained without taking dew thermal capacitance into account.

External convective heat transfer coefficients

The choice of external convective heat transfer coefficient model was important, since $\bar{h}_{conv}$ directly influenced condensation and evaporation rates in the roof condensation model. It was also preferable to use a model that could accurately account for the size of the roof surface, given the large roof areas under investigation. The ClearRoof model was applied to roof surfaces in the present work and the DOE-2 model was used for external vertical surfaces (i.e. walls).

Cases investigated

A case-study large-footprint shopping centre building was developed for the simulation study. It should be noted that no single building model can accurately represent the myriad different large-footprint buildings in existence, and that BPS results were found to be very sensitive to assumed building properties, operational schedules and loads, HVAC control and sizing strategies, etc. in the present investigation. An effort has been made to base the case study shopping centre on design standards and industry guidelines, where possible. However, the results presented here represent the performance of one typical building, and cannot necessarily be applied directly to all similar buildings.

Building details

The building model had plan dimensions of 350 m × 200 m and a double-pitched, low-angle roof, as shown in Figure 20. It was modelled with concrete walls, a metal deck roof and concrete slab on ground; 5% of the wall area was set as glazing and no roof glazing was included. The indoor space was divided into two storeys and one separate unconditioned roof cavity, each comprising a separate indoor zone.

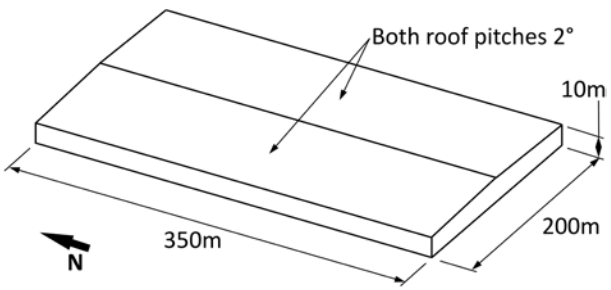

Figure 20: Diagram of the case-study building geometry.

The building fabric and construction details were set to meet minimum performance requirements outlined in the Australian National Construction Code of 2019 (NCC2019) for each climate investigated (Australian Building Codes Board, 2019). The thermal resistance (R-value) requirements for different climate zones can be found in Sections J1.3 and J1.5 of NCC2019. Additional simulations were run with a range of roof R-values, to investigate the importance of roof insulation in the relative benefits of cool roofs.

Very few previous studies were found that had quantified air infiltration rates for shopping centres. Jenkins (2008) noted that they could be expected to vary significantly over time and between different buildings; the author suggested values from 0.5 to 1.0 air changes per hour (ACH) at natural pressure. A value of 0.7 was set in the present investigation.

Roof radiative-optical properties

Three roof types were included in simulations: one representative of bare metal-coated steel sheet (e.g. zinc-aluminium coated steel), and two light-coloured painted steel sheet roofs, referred to herein as of 'light' and 'very light' roofs. Differences between the roofs are detailed in Table 3. In simulations incorporating the roof condensation model, the effective roof thermal emittance varied from the 'dry roof' values reported in Table 3 according to the amount of dew present on the roof.

It is important to note that the properties of roof materials can change significantly over time. The effect of such ageing depends on the local exposure conditions and the properties of the roof product, but light-coloured painted roofs have been shown to exhibit significant decreases in solar reflectance, even within the first three years of installation, and bare metal roofs tend to increase in thermal emittance (California Energy Commission, 2015; Paolini *et al.*, 2016; Cool Roof Rating Council, 2018). Factory-applied cool coatings, such as those on which the roofs in the present work were based, have been shown to change less over time than field-applied coatings, in the absence of biological growth (Sleiman *et al.*, 2011). However, the results of the present study should still be considered to represent building performance at a particular point in time, not a consistent performance that could be expected over the entire life of a roofing product.

Table 3: Radiative-optical properties of the roof products investigated.

Roof Type	Solar Reflectance	Thermal Emittance
Bare metal	0.67	0.3
Light-coloured	0.68	0.85
Very light-coloured	0.77	0.87

Building operation

Air conditioning and heating were used to maintain the indoor air temperature within 22.0–24.5°C between 7:00 and 18:00 every day, and no air conditioning was used outside of these periods. The majority of internal heat load magnitudes and schedules were defined as per the requirements for Class 6 buildings in NCC2019 (see Table 4). NCC2016 did not provide a maximum occupant density for such buildings, so a value from were Energy Action (2018) was used. The equipment load was set to 10 W m^{-2}, which is larger than the NCC2016 value of 5 W m^{-2}, to account for loads that are common in shopping centres but not within the typical

retail shop, e.g. vending machines, cooking equipment in food courts and any refrigeration in supermarkets that is not conditioned by rooftop units.

Table 4: Internal loads and schedules applied to the two case-study buildings.

Parameter	Setting
Lighting load [W m^{-2}]	22
Equipment load [W m^{-2}]	10
Maximum (inverse) occupant density [m^2 $person^{-1}$]	3
Occupant thermal load [W $person^{-1}$]	75 sensible, 55 latent
Lighting schedule	100% from 7:00 and 19:00, 10% otherwise
Equipment schedule	70% from 7:00 and 19:00, 10% otherwise
Occupancy schedule	Varies, maximum of 25% reached during 11:00–13:00
HVAC schedule	On between 7:00 and 18:00

HVAC systems

Detailed variable-air-volume HVAC systems were included in the building models (see Figure 4) based on design guidelines from ASHRAE Standard 90.1-2010 (ASHRAE 2010). They were comprised of one 'parallel fan-powered box' air handling unit per floor, each connected to four staged chillers and four gas boilers. Each simulation was run twice, once with air-cooled chillers and once with two wet cooling towers per chiller, to investigate whether above-roof temperature fields affect such systems differently.

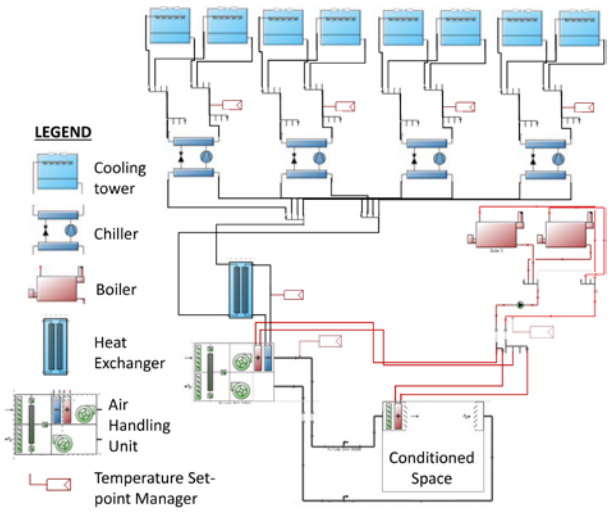

Figure 21: Schematic diagram of the detailed HVAC systems included in the building model; two such systems were used, one for each storey of the building. Simulations were also run with equivalent systems, except that the chillers were air-cooled (i.e. wet cooling towers were not included).

All HVAC components were automatically sized, based on simulations of 'extreme' summer and winter weeks specified in the weather data files. The nominal system cooling and heating capacities were set 1.15 and 1.25 times the maximum cooling and heating demands, respectively; these design factors were based on the recommendations of ASHRAE (DesignBuilder, 2018). Therefore, HVAC components were different sizes in each simulation and did not necessarily achieve the same coefficient of performance (COP) in each case.

Weather

Seven sets of weather conditions were simulated, representing typical conditions in major Australian cities located within climate zones 1–7, as described in the NCC2019 (see Figure 22 and Table 5). International Weather for Energy Calculation (IWEC) typical weather data files were used for all simulations except those of climate zones 3 and 4; IWEC weather data was not available for those locations, so reference meteorological year (RMY) data was used instead. It should be noted that some spatial variations in climate also exist within the climate zones, so the results presented here do not represent all Australian climates exactly.

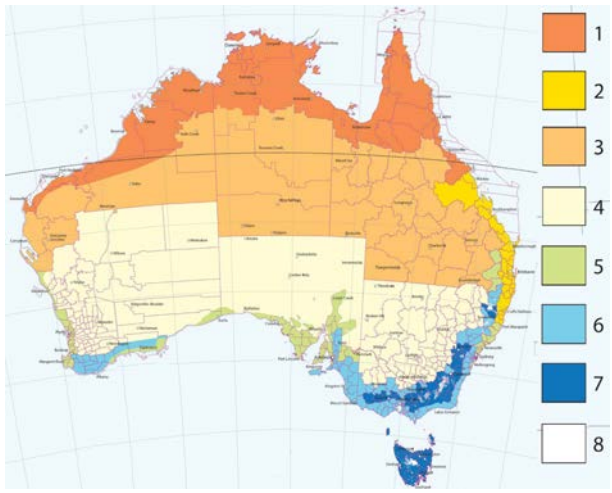

Figure 22: Australian climate zones, adapted from Australian Building Codes Board (2016); zones 1–7 were included in the BPS study.

Table 5: Australian cities that were used to represent each of the seven climate zones investigated.

Zone	Description	City
1	High humidity summer, warm winter	Darwin
2	Warm humid summer, mild winter	Brisbane
3	Hot dry summer, warm winter	Alice Springs
4	Hot dry summer, cool winter	Dubbo
5	Warm temperate	Sydney
6	Mild temperate	Melbourne
7	Cool temperate	Canberra

Results and discussion

Timestep sensitivity

Preliminary simulations were run with three different timestep values: 6, 2 and 1 min, all with the roof condensation model, bare metal roof, air-cooled chillers and weather data representing Sydney. Results from all three simulations were very similar. The RMS deviation between roof surface temperatures, dew mass loadings and latent heat fluxes obtained using timesteps of 6 min and 1 min were 0.30°C, 3.5 g m^{-2} and 8.0 W m^{-2}, respectively; between results obtained using timesteps of 2 min and 1 min, the corresponding RMS deviations were 0.025°C, 0.27 g m^{-2} and 0.71 W m^{-2}, respectively. Based on these indications of timestep sensitivity, it appeared timesteps as large as 6 min could be used without affecting results significantly. However, some signs of instability were observed in the spatially averaged roof surface temperatures obtained using a 6 and 2 min timesteps (see Figure 23). Such instability could cause large inaccuracies, so subsequent simulations were conducted with time steps of 1 min.

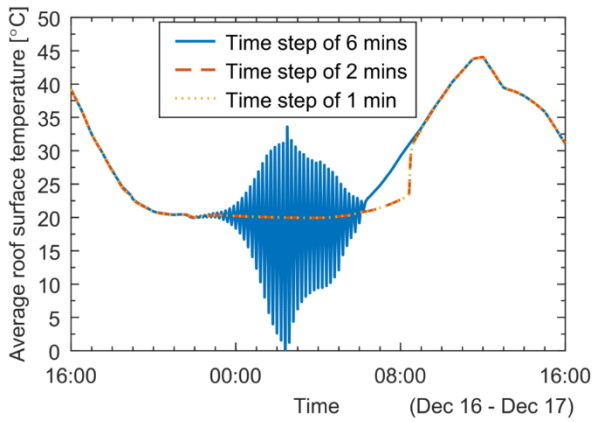

Figure 23: Example of unstable results produced using 6 min timesteps, compared to the corresponding results obtained with 2 and 1 min timesteps.

Influence of dew thermal capacitance

During the timestep sensitivity study, it was observed that a significant quantity (in the order of 100 g m^{-2}) of dew could accumulate on the roof under dynamic conditions. Since water has a relatively high specific heat capacity of approximately 4.2×10^3 J kg^{-1} K^{-1}, a dew mass loading of 150 g m^{-2} would have approximately one third of the thermal capacitance of the 0.5 mm-thick steel roof sheet. Therefore, it was considered prudent to assess whether the thermal capacitance of accumulated dew should be accounted for in simulations.

A simulation in which the roof sheet thermal capacitance was overridden at each timestep, to include the additional capacitance of any dew that was present, was compared to a simulation in which this was not done. Results from the two simulations were in close agreement; the RMS deviation between the simulated roof surface temperatures, dew mass loadings and latent heat fluxes were 0.029°C, 0.17 g m^{-2} and 0.56 W m^{-2}, respectively. Such small effects would not influence building performance significantly, so the effect of dew on roof thermal capacitance was not accounted for in subsequent simulations.

Dew condensation/evaporation dynamics

During approximately half of the nights simulated with Sydney weather, the roof surface temperature fell below the dewpoint temperature, which caused dew to form. On these occasions, dew continued to accumulate until the roof surface rose above the dewpoint temperature, at which time evaporation began. Typically, the dew was completely evaporated relatively quickly once evaporation began (see Figure 24); on average, it was completely evaporated within 2.2 h in simulations of Sydney. However, on a small number of days the solar heat flux did not raise the roof surface temperature high enough to completely evaporate all dew that was present, so the model predicted that some dew persisted over a period of several days (see Figure 25a).

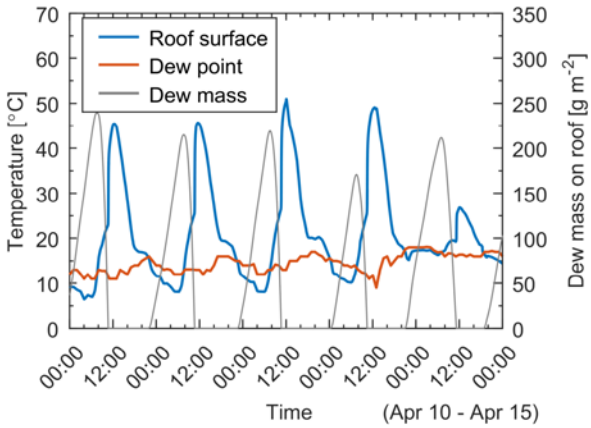

Figure 24: Example of the dynamic dew condensation/evaporation process over a period of 5 days, driven by the difference between roof surface temperature and dew-point temperature.

Dew effect on roof apparent thermal emittance

Over the course of the simulated year of Sydney weather, the bare metal roof apparent thermal emittance often rose to approximately 0.96 (see Figure 25b). Any dew mass loading greater than ~20 g m^{-2} would have this effect. Such conditions were typically reached in the early morning (~2:00–8:00). During these periods, the thermal performance of the bare metal roof and painted roofs would be quite similar, since both would have a high apparent thermal emittance, and differences in solar reflectance would have little effect due to the low solar heat flux. Conventional BPS practices (i.e. those ignoring the effects of dew) would not account for this phenomenon, so would be likely to overestimate the degree to which high-emissivity roofs (e.g. cool roofs) are colder than low-emissivity roofs (e.g. bare metal roofs) in the early morning.

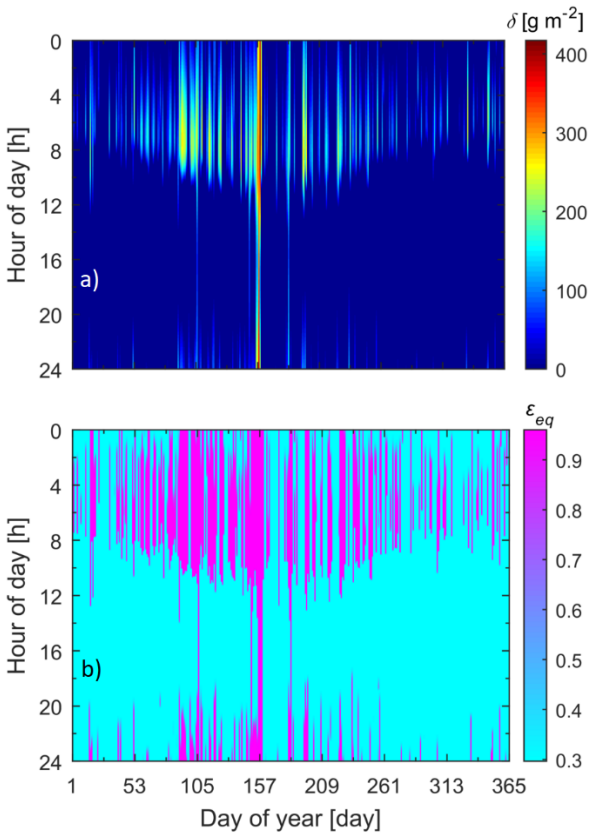

Figure 25: Apparent thermal emittance (ε_{eq}) of the bare metal roof during simulations of Sydney weather.

Dew effect on roof surface temperatures

The roof condensation model decreased the temperature of the bare metal roof by several degrees during many mornings in simulations (see Figures 26 and 27a), and tended to increase the very light roof temperature during the early morning and decrease it during the late morning (see Figure 27b). On some extreme occasions, the bare-metal roof surface temperature was reduced by over 15°C by dew. This occurred when the roof surface temperature was increasing rapidly in the morning (see Figure 26).

The effect of latent heat fluxes are clearly evident in results from the very light roof (Figure 27b); roof surface temperatures were typically driven warmer as dew condensed in the early morning, and colder as dew evaporated in the late morning (~8:00–10:00). In simulations of the bare metal roof, the effects of dew on roof apparent thermal emittance were much more pronounced, since the dry-roof emittance was much less than it was for the painted roofs. During the early morning, enhanced radiant heat exchange with the sky appears to have overpowered the warming effect of latent heat release during condensation, and the complementary effects of latent heat absorption and enhanced radiant heat exchange with the cold sky combined to drive the bare metal roof temperature down in the late morning.

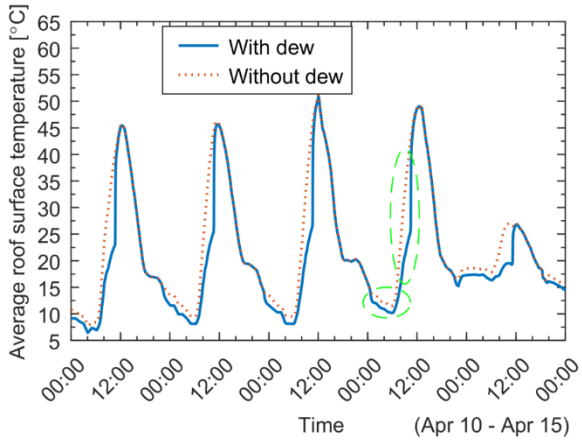

Figure 26: Comparison of roof surface temperatures simulated with and without the roof condcondensation model.

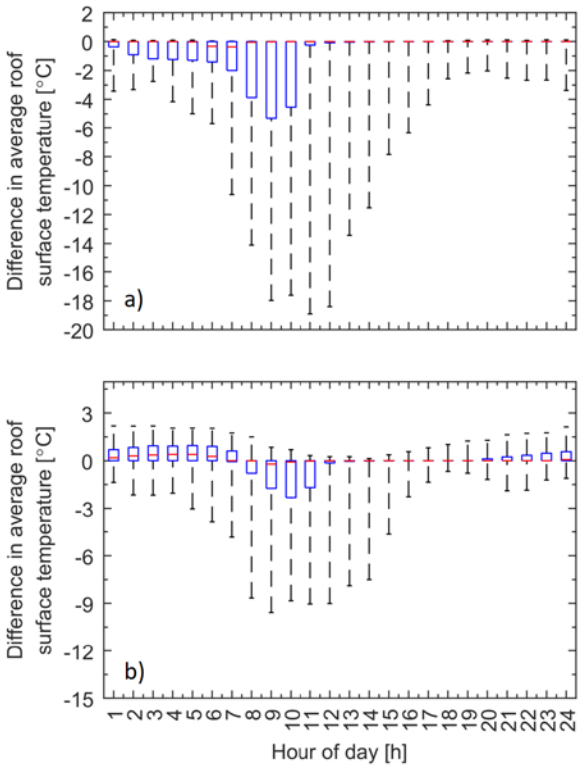

Figure 27: Difference between roof surface temperatures simulated with and without the condensation model, for the a) bare metal roof and b) very light roof in Sydney. Each red line indicates the distribution median, the blue 'boxes' bound the 2nd and 3rd quartiles, and the 'whiskers' extend to the minimum and maximum values within each distribution.

To investigate the relative importance of the two effects of dew (latent heat fluxes and modified roof thermal emittance) on roof surface temperatures, simulations were run in which only one of the two effects was imposed. The results revealed that, in simulations of the bare metal roof in Sydney, the effect of dew on the roof apparent thermal emittance was the primary cause of changes in roof surface temperature (see Figure 28).

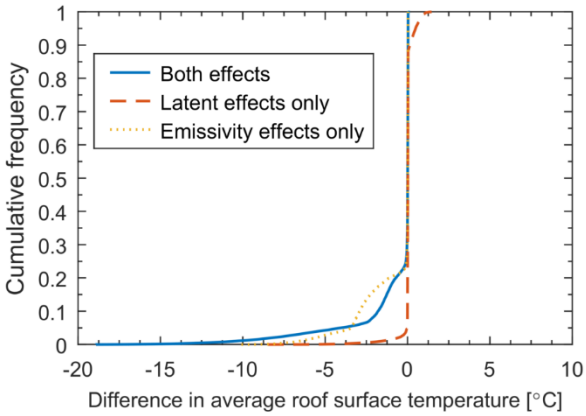

Figure 28: Effects of dew on the bare metal roof temperature, when taking either the latent heat effects, emissivity effects, or both effects into account.

Above-roof air temperatures

Corrected HVAC inlet temperatures (T_{HVAC}) calculated by the above-roof temperature model typically differed from the ambient air temperature (T_{amb}) by 0–1.2°C (see Figure 29). Air close to all three roofs was typically driven hotter than T_{amb} during daylight hours, when the sun heated the roof surfaces, and colder than T_{amb} at night-time, when radiant heat exchange with the sky drove T_s below T_{amb}. The light and very light roofs tended to remain colder than the bare metal roof due to their higher solar reflectance and thermal emittance, so T_{HVAC} also tended to be colder in simulations of those roofs. These results were commensurate with experimentally measured and simulated values from project RP1037 (Green *et al.*, 2018).

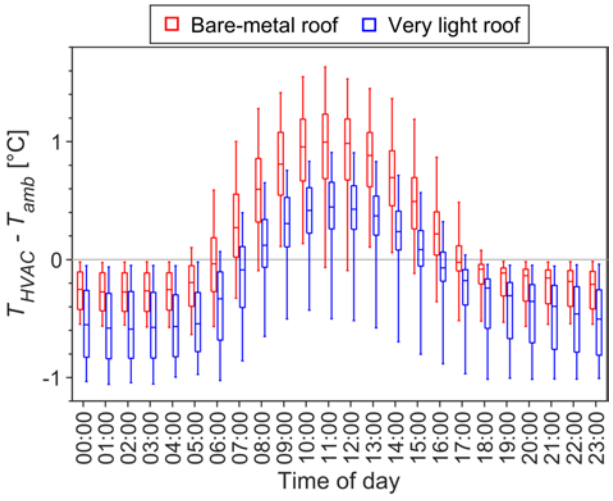

Figure 29: Effect of the above-roof temperature model on HVAC inlet temperatures, in simulations of Sydney, neglecting the effects of dew. Each 'box' and set of 'whiskers' represent the distribution of values recorded during the specified hour of day throughout the entire year-long simulation.

Annual cooling and heating requirements

The above-roof temperature model increased annual cooling requirements by 4–23% and decreased annual heating requirements by 6–12% for the building with a bare metal roof (see Figure 30). The roof condensation model had a much smaller effect on the annual thermal HVAC loads (less than 0.6% and 2.1% for cooling and heating, respectively).

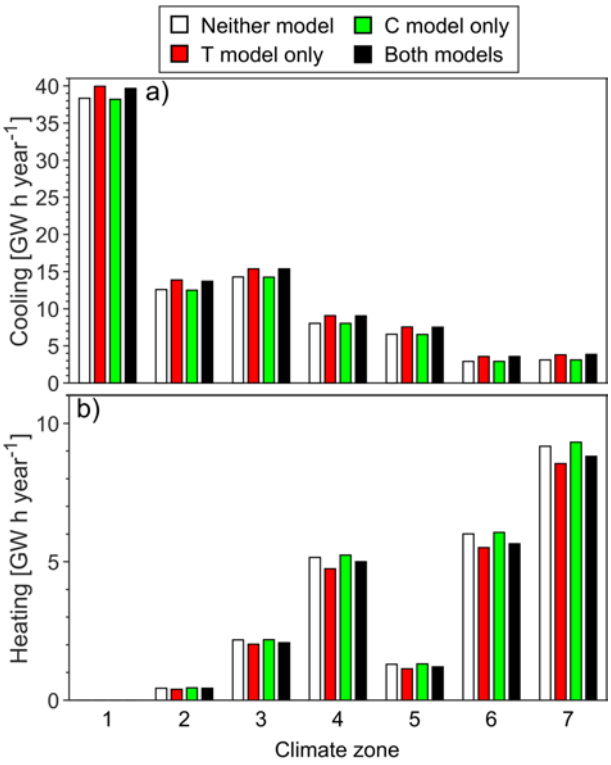

Figure 30: Annual a) cooling and b) heating requirements of the building with bare metal roof. Results are presented from simulations with the above-roof temperature model (T model), roof condensation model (C model), both models, and neither model.

The effect of the two models on thermal loads in simulations of light and very light roofs was similar to that reported for the bare metal roof, above, except that above-roof temperatures tended to have less of an effect and dew tended to have a larger effect. In simulations of the two painted roofs, the above-roof temperature model caused annual cooling to increase by 1.3–16% and annual heating to either decrease or increase by 0.4–4.9%. The roof condensation model caused annual cooling to increase by 0.8–2.4% and annual heating to decrease by 1.4–4.8%.

Annual electricity and gas consumption

The annual HVAC electricity and gas consumption calculated in simulations of the building with air-cooled chillers are presented in Figure 31. Chillers with wet cooling towers typically performed with higher COPs than the corresponding air-cooled chillers, leading to a reduction in total annual HVAC electricity consumption of 11–31% (and no effect on gas consumption).

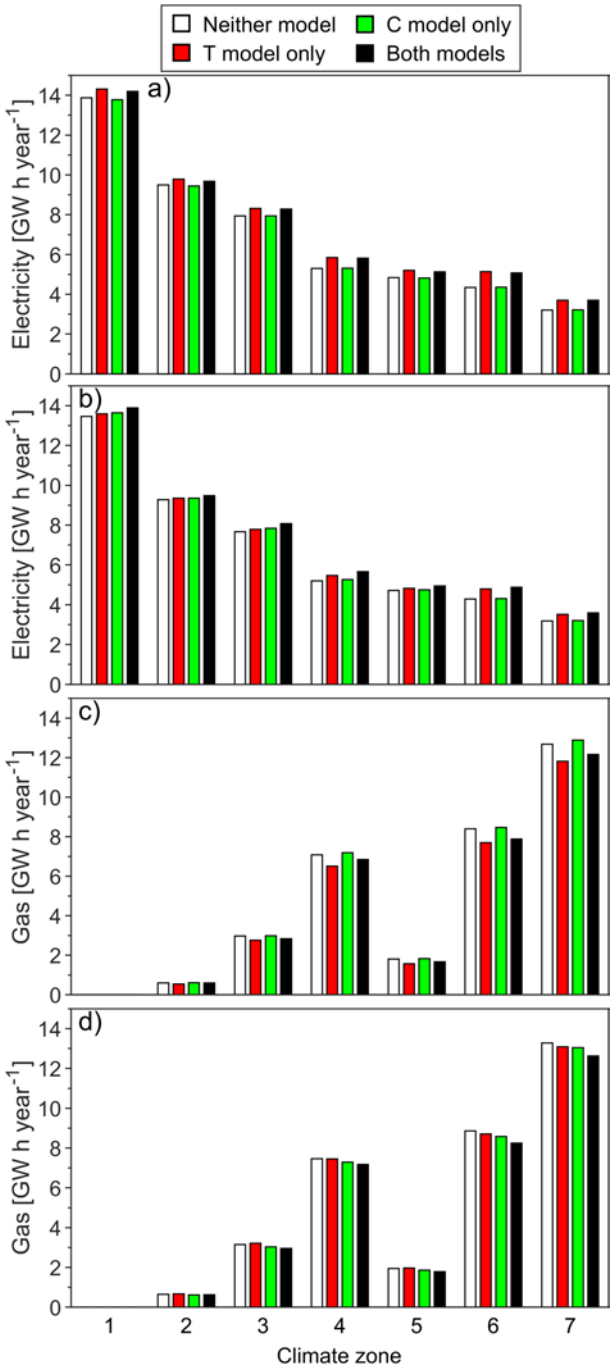

Figure 31: Annual HVAC electricity (a-b) and gas (c-d) consumption of the building with air-cooled chillers and either a bare metal roof (a, c) or very light roof (b, d). Results are presented from simulations with the above-roof temperature model (T model), roof condensation model (C model), both models, and neither model.

The effects of above-roof air temperatures and dew on electricity and gas consumption were generally similar to their effect on cooling and heating loads. The above-roof temperature model tended to increase HVAC electricity consumption and decrease gas consumption, and affected the building with bare metal roof more than those with painted roofs. The roof condensation model typically had very small effect in simulations of the bare metal roof, and tended to increase electricity consumption slightly and decrease gas consumption in cases involving the light and very light roofs.

The combined effects of the two models when implemented together did not equate to the sum of effects caused by each model individually. The roof condensation model influenced roof surface temperatures and, thereby, above-roof air temperatures, so the effects of dew were amplified by the above-roof temperature model. Typically, the two models had opposing effects on HVAC energy consumption in cases with the bare metal roof, and complimentary effects in cases with the light and very light roofs. These trends can be understood by considering that the bare metal roof was typically cooled by dew during mornings, so T_{HVAC} was lower, mitigating above-roof temperature effects (which would otherwise tend to increase HVAC energy consumption when cooling was required and decrease it when heating was required). In cases with either of the painted roofs, the roof condensation model had a relatively large effect on thermal loads, which caused changes in electricity and gas consumption that complemented the effects of above-roof air temperatures.

Cool roof electricity savings and gas penalties

In order to quantify the operational savings attributable to cool roofs in the cases investigated, simulations of the very light roof (a cool roof) and the bare metal roof (a typical 'non-cool' roof) were compared. Figure 32 presents this comparison for buildings with air-cooled chillers, and Figure 33 shows the same results for buildings with wet cooling towers. The magnitude of electricity savings and gas penalties corresponded quite closely to the annual HVAC electricity and gas consumption, respectively. Cool roof savings/benefits obtained with air-cooled chillers were very similar to those obtained with wet cooling towers, but were slightly higher in some cases.

Above-roof air temperatures and dew both had a large effect on the electricity savings and gas penalties attributable to the cool roof. The two models had opposing effects on the savings/penalties in all cases; the above-roof temperature model consistently increased electricity savings and gas penalties, and the roof condensation model consistently decreased them. When both models were implemented their combined effect varied; gas penalties were reduced in all climates, as were electricity savings in hot climates (zones 1–3), with the exception of climate zone 2 when wet cooling towers were included, and electricity savings were increased in temperate climates (zones 4–7).

The magnitude of effect that the models had on predicted electricity savings and gas penalties demonstrates the importance of these phenomena in the performance of technologies like cool roofs. If conventional BPS practices were adhered to, both above-roof temperature and dew effects would be neglected. While such simplifications would have only affected annual energy consumption by several percent in the cases investigated here, the relative performance of a cool roof compared to a 'non-cool' roof could have

been miscalculated by a much larger fraction. In the cases investigated here, the effects of above-roof air temperatures and dew on annual savings/penalties tended to cancel each other out, to a degree. However, simulations with different building geometries, construction details, internal loads, usage schedules and/or climates could be affected differently.

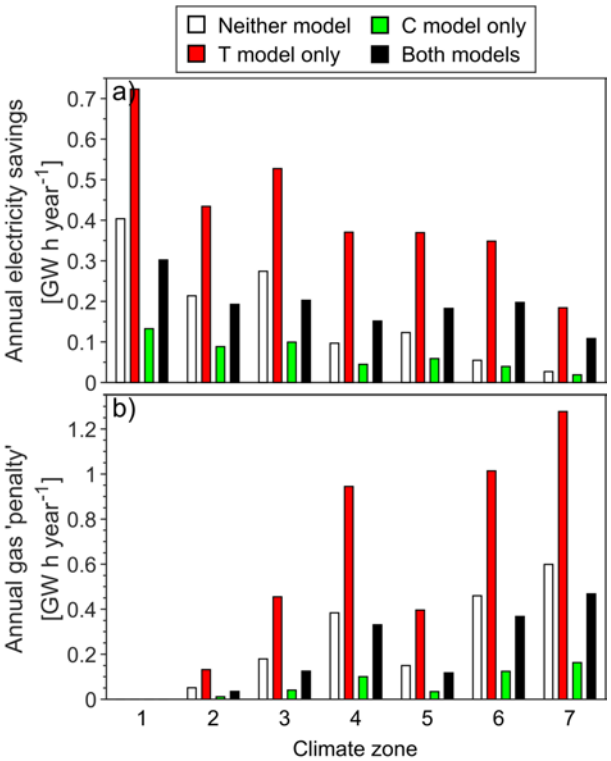

Figure 32: Annual a) electricity savings and b) gas 'penalties' attributable to the use of the very light roof rather than the bare metal roof, for the building with air-cooled chillers. Results are presented from simulations with the above-roof temperature model (T model), roof condensation model (C model), both models, and neither model.

Sensitivity to ceiling insulation thickness

Results from simulations with different amounts of ceiling insulation were compared, to investigate how each model affected results with roof R-values higher or lower than the values specified in NCC2019. Such cases have relevance to existing buildings that do not meet current building code requirements, and to buildings with more ceiling/roof insulation than is required. Results from this comparison also provided additional insight into how each model influenced the simulated building.

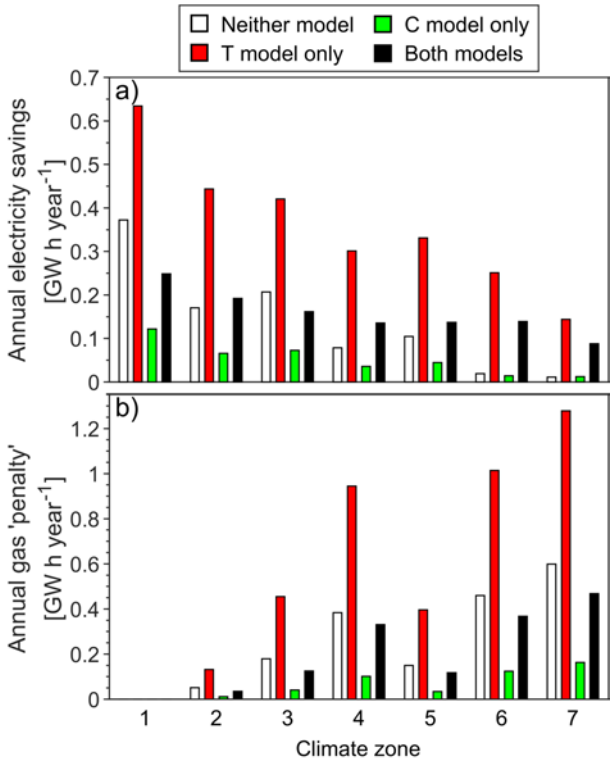

Figure 33: Annual a) electricity savings and b) gas 'penalties' attributable to the use of the very light roof rather than the bare metal roof, for the building with water-cooled chillers. Results are presented from simulations with the above-roof temperature model (T model), roof condensation model (C model), both models, and neither model.

HVAC electricity savings and gas penalties attributable to the cool roof both tended to increase with decreasing roof R-value (see Figure 34), since differences in roof surface temperature had a larger effect on the heat flux through the roof structure. In most cases, the two models affected annual energy savings/penalties by a similar magnitude, regardless of the roof R-value. However, when very little roof insulation was included, reducing the total roof R-value to ~0.5, the roof condensation model reduced gas penalties by a much larger amount (see Figure 34b). Such a trend could be explained by the effects of dew on roof surface temperatures, which can influence HVAC energy consumption via two pathways: i) driving heat transmission through the roof structure, and ii) influencing air temperatures at the inlet to rooftop HVAC equipment. When less ceiling insulation is installed, the first of these pathways is enhanced, so the effects of dew are also enhanced. By contrast, the above-roof temperature model provides a means to include the second pathway in simulations, but does not affect temperatures within the simulation directly.

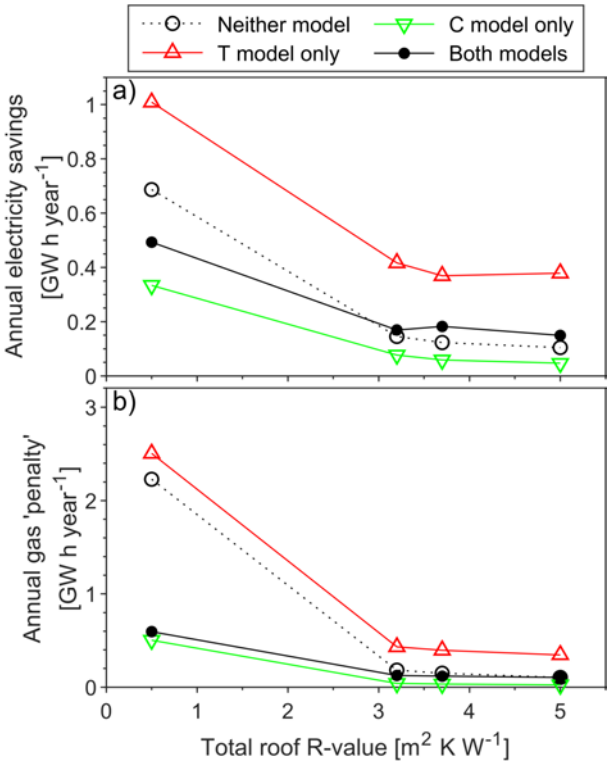

Figure 34: Influence of ceiling insulation on the annual HVAC electricity savings and gas 'penalties' attributable to the use of the very light roof rather than the bare metal roof in Sydney. Results are presented from simulations with the above-roof temperature model (T model), roof condensation model (C model), both models, and neither model.

Economic analysis

The net effect of electricity savings and gas penalties on the overall operational savings and emissions abatement attributable to cool roofs depends on the unit financial costs and greenhouse gas emission factors of gas and electricity. To investigate these dependencies for the cases investigated, a cost-benefit analysis and greenhouse gas emissions abatement estimate were conducted.

Operational cost savings

In order to compare electricity savings and gas penalties on a financial basis, each value needed to be multiplied by a unit cost. In reality, electricity and gas pricing structures are often complex. Unit prices can vary according to time of use, and other tariffs associated with the customer peak demand may also be applied. The scope of the current project did not permit time for a comprehensive analysis of the impact of pricing structures on the operational saving brought about by cool roofs. The analysis presented here has been based on single unit costs for both gas and electricity, which provided an indicative range of results for the building investigated. To fully explore the cost savings caused by cool roofs accurately, the hourly results of BPS would need to be analysed alongside the energy supply contracts in place for a particular building.

A range of electricity and gas unit costs were included in the analysis, in order to provide results that are widely applicable, despite the significant variations in electricity and gas costs across different Australian jurisdictions, and the high probability that such costs will change significantly over time. The ratio of electricity price to gas price (both expressed in units of \$ kW^{-1} h^{-1}), ω, was used to relate the two unit prices in graphs.

Figure 35 presents the running cost savings per unit floor area attributable to the use of the very light roof rather than the bare metal roof (see definitions of these roofs in the previous section of this report) on the case-study shopping centre building. In order to quantify the effects of the above-roof temperature and roof condensation models, results from simulations conducted with both models and those conducted with neither model have both been plotted.

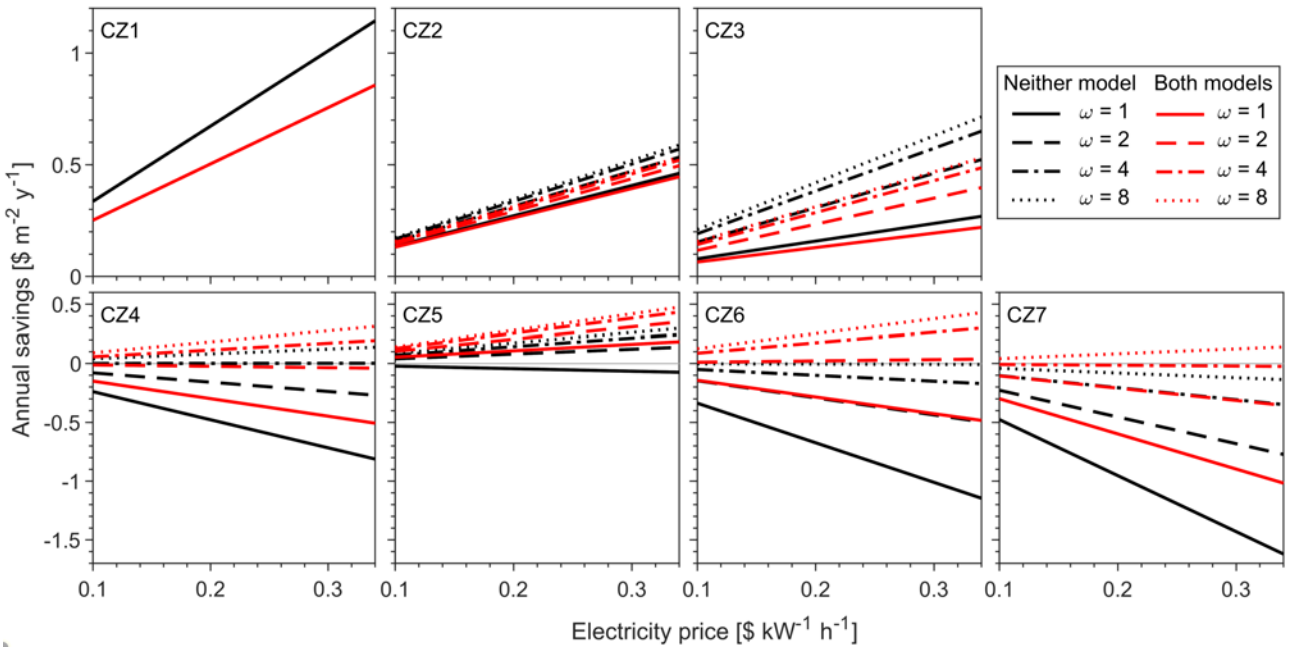

Figure 35: Annual HVAC running cost savings per unit floor area attributable to the use of the very light roof rather than the bare metal roof, calculated for the case-study shopping centre building with air-cooled chillers in seven climate zones (CZ1–7), for different electricity-gas cost ratios (ω), and with both the above-roof temperature and roof condensation models, or with neither model.

A net saving in running costs was calculated for all cases in climate zones 1, 2, 3 and 5. The magnitude of cost saving increased with ratio of unit costs for electricity and gas (ω), and with the magnitude of those unit costs for a given value of ω. In climate zones 4, 6 and 7, the cool roof was predicted to either decrease or increase running costs, depending on the value of ω. The magnitude of predicted savings/losses was significant in most cases. An annual saving per unit floor area of 0.1 [\$ m^{-2} y^{-1}] would amount to a total operational saving of \$280,000 for the case-study building considered here, if it is assumed that the roof products have a service life of 20 years. The operational saving over the service life of the roof could be compared to the upfront cost difference between the different roof types to help determine which is most cost-effective.

The combined effect of the above-roof temperature and roof condensation models was to increase HVAC running cost savings in the four climate zones where electricity savings had been increased (4–7). In other climates, the combined effect of the models depended

on ω, since gas penalties had been decreased but electricity savings had also been decreased, resulting in opposing effects on running cost savings.

It is important to note that the results presented here do not necessarily apply to all large-footprint buildings in the climate zones specified. The cost savings attributable to cool roofs is likely to vary significantly, depending on the building construction details, usage, HVAC equipment, and location. Furthermore, the ageing of roof materials and changes in electricity and gas prices are likely to change the performance of cool roofs over time. However, the results presented here for the case-study shopping centre building at one point in time do demonstrate the importance of dew and above-roof air temperature effects in assessments of this type. If these phenomena had not been included in the analyses presented here, the operational savings attributable to the cool roof would have been miscalculated by over 50% in many cases, and a net loss could have been predicted in climate zones 4, 6 or 7, when in fact a net saving had been possible.

Greenhouse gas emissions abatement

The abatement of greenhouse gas emissions was estimated using emission factors from the Australian Government July 2017 National Greenhouse Accounts Factors report (Australian Government Department of the Environment and Energy and Energy, 2017). As had been the case for electricity and gas unit prices, the analysis was highly sensitive to the emissions factors chosen, and significant variations in emissions factors existed within Australia. For these reasons, a range of electricity emissions factors were included in the analysis. The emissions factor for natural gas was much more consistent within Australia, so it was fixed at the national average specified in the National Greenhouse Accounts Factors report (0.214 kg CO_2-e kW^{-1} h^{-1}).

Figure 36 presents the estimated greenhouse gas emissions abatement attributable to the very light roof, as compared to the bare metal roof, for the case-study shopping centre building with air-cooled chillers in all seven climate zones. Negative abatements (i.e. increased emissions) were possible in all climate zones where heating (using gas) was required, given very low electricity emission factors. However the 'break even' point (above which the cool roof was predicted to cause a net decrease in emissions) was very low in climate zones 1, 2, 3 and 5, so the cool roof would reduce emissions in those climates unless electricity was available with an extremely low emission factor (≲0.15 kg CO_2-e kW^{-1} h^{-1}).

The effect of the above-roof temperature and roof condensation models on greenhouse gas emissions abatements was similar to the effect they had on operational cost savings. In climate zones 4–7, the models increased the electricity savings and decreased the gas penalties attributable to the cool roof, which produced a net decrease in predicted greenhouse gas emissions (i.e. increase in predicted abatement). In climate zones 2 and 3, the effect of dew and above-roof air temperatures depended on the electricity emission factor, and in climate zone 1 the models reduced electricity savings, thereby reducing predicted emissions abatements. The high sensitivity of greenhouse gas emissions abatement estimates to dew and above-roof air temperature fields is clearly visible in Figure 36. For instance, neglecting these factors in the present cases would have caused the cool roof to appear inappropriate for climate zones 6 and 7, when it could be beneficial in reality, depending on the electricity emission factor.

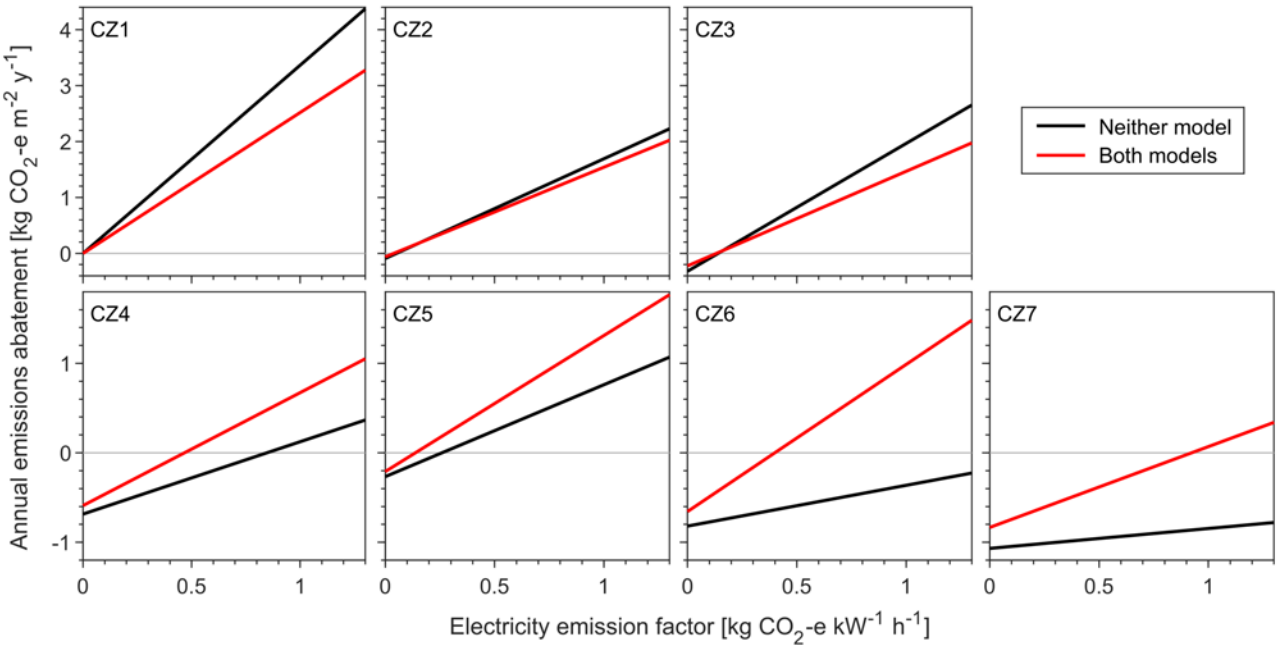

Figure 36: Annual greenhouse gas emissions abatement per unit floor area due changes in HVAC electricity and gas consumption if a very light roof were installed rather than a bare metal roof. Results are presented for the case-study shopping centre building with air-cooled chillers in seven climate zones (CZ1–7), with both the above-roof temperature and roof condensation models, and with neither model.

Conclusion

To the authors' knowledge, this has been the first study to publish such in-depth analysis of the effects of i) dew and ii) near-roof air temperatures on the energy consumption of large-footprint buildings. Detailed literature reviews, theoretical analysis, experimental measurements and simulations have been used to quantify these effects for case-study shopping centre buildings with different cool and 'non-cool' roofs. Both effects were found to be significant in the cases investigated, especially in comparisons between the simulated performance of a cool roof and a bare metal-coated steel roof. If dew and above-roof temperature fields had been neglected in these cases, the effects of the cool roof on annual HVAC electricity and gas consumption would have been miscalculated by 11–75% (42% on average) and 16–46% (31% on average), respectively. There is a significant probability that such large errors could cause cool roofs to be erroneous deemed cost-effective or not (in terms of financial cost and/or environmental impact). Therefore, both dew and above-roof air temperatures should be considered in simulation studies that compare cool roofs to other roofing products for large-footprint buildings.

The roof condensation model that has been developed can predict dew condensation and evaporation on a roof external surface in dynamic BPS. The latent heat released/absorbed through these processes can thereby be applied in the roof surface energy balance calculations, and by tracking the dew film thickness over time the effect of accumulated dew on the roof thermal emittance can also be accounted for. In the simulations reported here, the relative importance of i) latent heat absorption/release and ii) changes in apparent thermal emittance was found to depend on the type of roof; changes in thermal emittance had a larger effect on roof surface temperature in simulations of the low-emittance bare metal roof than for painted roofs. The results of the present study indicate that both effects should be included if the influence of dew on roof temperature is to be accurately modelled.

The above-roof temperature model described in this report is a revised version of that developed in project RP1037 (Green *et al.*, 2018). An improved statistical fit to experimental data has reduced the RMS deviation between model predictions and the RP1037 near-roof air temperature measurements from 0.83°C to 0.56°C in unstable conditions (i.e. when the roof surface is hotter than the ambient air temperature). This change is likely to have had a relatively small effect on BPS results, but the values presented here should be considered to supersede those in the RP1037 final report.

The range of weather conditions and building types that the above-roof temperature model can currently be applied to with confidence has also been quantified. It was found that the cases simulated here did not extend significantly beyond the conditions on which the model was based, so application of the model in those cases appears to be justified. Future users of the model should understand its limitations, as outlined in this report, and further comparison of the model with experimental data would be highly valuable.

Several important simplifications were made in the present study:

1. Only one case-study building was investigated in the BPS study and economic analysis. Results were found to be highly sensitive to modelling assumptions (e.g. building construction details, internal loads, usage schedules, HVAC system design, etc.), so the results presented here should not be considered to represent all large-footprint buildings.
2. Roof radiative-optical properties are known to change over time. Such 'ageing' was not taken into account in the present work, so the results presented here are not necessarily accurate for the entire service life of a roof.
3. The current implementation of the roof condensation model: i) assumes that dew forms a continuous film of uniform thickness, and ii) does not model water condensation on the roof internal surface.
4. Cool roof performance was compared to a bare metal-coated steel roof, which is a conventional 'non-cool' roofing product in Australia. In other regions of the world, comparisons between cool roofs and 'non-cool' high-emittance roofs (e.g. asphalt or dark painted roofs) may be more relevant.
5. Effects of above-roof air temperatures and dew on heating and cooling peak loads were not analysed in this study. If these effects were taken into account when selecting the size of HVAC equipment for a building, upfront cost savings and greenhouse gas emissions abatements may be achievable.

Further investigation into these issues would assist in further understanding the true benefits of cool roofs, and the importance of the physical phenomena investigated here in assessments of such benefits.

References

Ambrose, D. and Karagiozis, A. (2007) 'Pressure Equalized Insulated Glass Units in Exterior Building Envelopes', *ASHRAE*.

ASHRAE (2009) *ASHRAE Handbook: Fundamentals*. Atlanta, GA, USA: American Society of Heating, Refrigeration and Air-Conditioning Engineers.

Australian Building Codes Board (2016) 'National Construction Code'. Available at: http://www.abcb.gov.au.

Australian Building Codes Board (2019) 'National Construction Code - Volume 1'.

Australian Government Department of the Environment and Energy and Energy, D. of the E. and (2017) *National Greenhouse Accounts Factors*. July 2017.

Bassett, M. R. and Trethowen, H. A. (1984) 'Effect of Condensation on Emittance of Reflective Insulation', *Journal of Thermal Insulation*. Sage PublicationsSage CA: Thousand Oaks, CA, 8(2), pp. 127–135. doi: 10.1177/109719638400800207.

Bergman, T. *et al.* (2011) *Fundamentals of heat and mass transfer*. 7th edn. Jefferson, USA: John Wiley & Sons.

Beysens, D. *et al.* (2005) 'Measurement and modelling of dew in island, coastal and alpine areas', *Atmospheric Research*. Elsevier, 73(1–2), pp. 1–22. doi: 10.1016/J.ATMOSRES.2004.05.003.

Beysens, D. *et al.* (2006) 'Application of passive radiative cooling for dew condensation', *Energy*. Pergamon, 31(13), pp. 2303–2315. doi: 10.1016/J.ENERGY.2006.01.006.

Blocken, B., Tominaga, Y. and Stathopoulos, T. (2013) 'CFD simulation of micro-scale pollutant dispersion in the built environment', *Building and Environment*, 64(0), pp. 225–230. doi: http://dx.doi.org/10.1016/j.buildenv.2013.01.001.

Bloudek, K. (1992) *Building physics II - 1. Calculation methods*, *CVUT Prague*.

California Energy Commission (2015) '2016 Building Energy Efficiency Standards for Residential and Nonresidential Buildings - Title 24', *Part 6*.

Carter, G. (2011) 'Issues and solutions to more realistically simulate conventional and cool roofs', in *Proceedings of Building Simulation 2011: 12th Conference of international building performance simulation association (IBPSA). Sydney, 14–16 November 2011*.

Carter, G. and Kosasih, B. (2015) 'Not so cool roofs', in *AIRAH's Future of HVAC 2015 Conference*. Melbourne, Australia.

Castro, I. P. and Robins, A. G. (1977) 'The flow around a surface-mounted cube in uniform and turbulent streams', *Journal of Fluid Mechanics*. 04/11. Cambridge University Press, 79(2), pp. 307–335. doi: 10.1017/S0022112077000172.

Çengel, Y. A. and Boles, M. A. (2002) *Thermodynamics : an engineering approach*.

Clear, R. D., Gartland, L. and Winkelmann, F. C. (2003) 'An empirical correlation for the outside convective air-film coefficient for horizontal roofs', *Energy and Buildings*, 35(8), pp. 797–811. doi: https://doi.org/10.1016/S0378-7788(02)00240-2.

Cool Roof Rating Council (2018) *Product rating program manual CRRC-1*.

Costanzo, V. *et al.* (2014) 'Proper evaluation of the external convective heat transfer for the thermal analysis of cool roofs', *Energy and Buildings*, 77, pp. 467–477. doi: http://dx.doi.org/10.1016/j.enbuild.2014.03.064.

DesignBuilder (2018) 'DesignBuilder Software Limited'. Available at: http://www.designbuilder.co.uk.

Downing, H. D. and Williams, D. (1975) 'Optical constants of water in the infrared', *Journal of Geophysical Research*. John Wiley & Sons, Ltd, 80(12), pp. 1656–1661. doi: 10.1029/JC080i012p01656.

Duffie, J. A. and Beckman, W. A. (2013) *Solar engineering of thermal processes*. 4th edn. New York, USA: John Wiley and Sons.

Energy Action (2018) *Building Code Energy Performance Trajectory Project*.

EnergyPlus (2010) 'EnergyPlus Engineering Reference: The Reference to EnergyPlus Calculations.' US Department of Energy.

Essah, E. A. *et al.* (2009) 'Condensation and moisture transport in cold roofs: effects of roof underlay', *Building Research & Information*. Routledge , 37(2), pp. 117–128. doi: 10.1080/09613210802645973.

Gebhart, B. *et al.* (1988) *Buoyancy-induced flows and transport*. New York: Hemisphere Publishing Corporation.

Green, A. *et al.* (2018) *Driving Increased Utilisation of Cool Roofs on Large-Footprint Buildings*.

Hale, G. M. and Querry, M. R. (1973) 'Optical Constants of Water in the 200-nm to 200-μm Wavelength Region', *Applied Optics*. Optical Society of America, 12(3), p. 555. doi: 10.1364/AO.12.000555.

Holck, O. and Svendsen, S. (2004) 'Modeling of Microclimates', *Performance and Durability Assessment*. Elsevier, pp. 297–326. doi: 10.1016/B978-008044401-7/50023-7.

Hosseini, S. A., Kermani, A. M. and Arabhosseini, A. (2019) 'Experimental study of the dew formation effect on the performance of photovoltaic modules', *Renewable Energy*. Elsevier Ltd, 130, pp. 352–359. doi: 10.1016/j.renene.2018.06.063.

Ilse, K. *et al.* (2019) 'Dew as a Detrimental Influencing Factor for Soiling of PV Modules', *IEEE Journal of Photovoltaics*, 9(1), pp. 287–294. doi: 10.1109/JPHOTOV.2018.2882649.

Keller, J. (1985) 'Characterization of the Thermal Performance of Uncovered Solar Collectors by

Parameters Including the Dependence on Wind Velocity', in *Workshop on solar assisted heat pumps with ground coupled storage, Vienna, Austria, 8 May 1985*. Available at: https://www.osti.gov/etdeweb/biblio/7837131 (Accessed: 21 February 2019).

Krauter, S. (2004) 'Increased electrical yield via water flow over the front of photovoltaic panels', *Solar Energy Materials and Solar Cells*. North-Holland, 82(1–2), pp. 131–137. doi: 10.1016/J.SOLMAT.2004.01.011.

Laboratory, L. B. (1994) *DOE2 engineers manual, Version 2.1A*. Los Alamos, NM.

Lee, S. W., Lim, C. H. and Salleh, E. @ I. Bin (2016) 'Reflective thermal insulation systems in building: A review on radiant barrier and reflective insulation', *Renewable and Sustainable Energy Reviews*. Pergamon, 65, pp. 643–661. doi: 10.1016/J.RSER.2016.07.002.

Leonard, Tim and Leonard, Tony (2006) 'Stay Cool: A roof system on a Minnesota building demonstrates energy-saving technology', *Professional Roofing*. Available at: http://www.professionalroofing.net.

Maestre-Valero, J. F., Martin-Gorriz, B. and Martínez-Alvarez, V. (2015) 'Dew condensation on different natural and artificial passive surfaces in a semiarid climate', *Journal of Arid Environments*. Academic Press, 116, pp. 63–70. doi: 10.1016/J.JARIDENV.2015.02.002.

Mao, G. and Kurata, K. (1998) 'Changes in Porosity and Longwave Characteristics of Row Cover Non-woven Fabrics due to Condensation.', *Journal of Agricultural Meteorology*. The Society of Agricultural Meteorology of Japan, 54(2), pp. 161–165. doi: 10.2480/agrmet.54.161.

Martin, M. and Berdahl, P. (1984) 'Characteristics of infrared sky radiation in the United States', *Solar Energy*. Pergamon, 33(3–4), pp. 321–336. doi: 10.1016/0038-092X(84)90162-2.

Mcadams, W. H. (1942) *Heat transmission*. New York: McGraw-Hill.

Mirsadeghi, M. *et al.* (2013) 'Review of external convective heat transfer coefficient models in building energy simulation programs: Implementation and uncertainty', *Applied Thermal Engineering*, 56(1), pp. 134–151.

Mitchell, J. W. (1976) 'Heat transfer from spheres and other animal forms', *Biophysical Journal*. Cell Press, 16(6), pp. 561–569. doi: 10.1016/S0006-3495(76)85711-6.

Monteith, J. L. and Unsworth, M. H. (2013) *Principles of environmental physics*. 4th edn. London: Edward Arnold.

Paolini, R. *et al.* (2014) 'Effect of ageing on solar spectral reflectance of roofing membranes: Natural exposure in Roma and Milano and the impact on the energy needs of commercial buildings', *Energy and Buildings*, 84, pp. 333–343.

Paolini, R. *et al.* (2016) 'An accelerated procedure to mimic weathering and soiling of building envelope materials in European urban areas', in *Fourth International Conference on Countermeasures to Urban Heat Island*. National University of Singapore, pp. 1–11.

Pieters, J. G., Deltour, J. M. J. J. and Debruyckere, M. J. G. (1995) 'Onset of Condensation on the Inner and Outer Surface of Greenhouse Covers during Night', *Journal of Agricultural Engineering Research*. Academic Press, 61(3), pp. 165–171. doi: 10.1006/JAER.1995.1043.

Piscia, D. *et al.* (2012) 'A CFD greenhouse night-time condensation model', *Biosystems Engineering*. Academic Press, 111(2), pp. 141–154. doi: 10.1016/J.BIOSYSTEMSENG.2011.11.006.

Pisello, A. L., Santamouris, M. and Cotana, F. (2013) 'Active cool roof effect: impact of cool roofs on cooling system efficiency', *Advances in building energy research*, 7(2), pp. 209–221.

Richards, K. (2009) 'Adaptation of a leaf wetness model to estimate dewfall amount on a roof surface', *Agricultural and Forest Meteorology*, 149(8), pp. 1377–1383. doi: 10.1016/j.agrformet.2009.02.014.

Richards, P. J. *et al.* (2007) 'Wind-tunnel modelling of the Silsoe Cube', *Journal of Wind Engineering and Industrial Aerodynamics*, 95(9), pp. 1384–1399. doi: http://dx.doi.org/10.1016/j.jweia.2007.02.005.

Robinson, H. E., Cosgrove, L. A. and Powell, F. J. (1957) *Thermal resistance of airspaces and fibrous insulations bounded by reflective surfaces - Building Materials and Structures Report 151*.

Sidran, M. (1981) 'Broadband reflectance and emissivity of specular and rough water surfaces', *Applied Optics*. Optical Society of America, 20(18), p. 3176. doi: 10.1364/AO.20.003176.

Simpson, A., Castles, G. and O'Connor, D. E. (1992) 'Condensation, heat transfer and ventilation processes in flat timber-frame cold roofs', *Building Services Engineering Research and Technology*. Sage PublicationsSage CA: Thousand Oaks, CA, 13(3), pp. 133–145. doi: 10.1177/014362449201300302.

Sleiman, M. *et al.* (2011) 'Soiling of building envelope surfaces and its effect on solar reflectance—Part I: Analysis of roofing product databases', *Solar Energy Materials and Solar Cells*, 95(12), pp. 3385–3399.

Sleiman, M. *et al.* (2014) 'Soiling of building envelope surfaces and its effect on solar reflectance–Part II: Development of an accelerated aging method for roofing materials', *Solar Energy Materials and Solar Cells*, 122, pp. 271–281.

Tiwari, G. N., Kumar, A. and Sodha, M. S. (1982) 'A review—Cooling by water evaporation over roof', *Energy Conversion and Management*. Pergamon, 22(2), pp. 143–153. doi: 10.1016/0196-8904(82)90036-X.

Tywoniak, J. (1999) 'EFFECT OF LONGWAVE RADIATION IN COLD ROOFS-REMARKS ON SIMULATIONS', in *Proceedings of the International Building Performance Simulation Association*.

Vargaftik, N. B., Volkov, B. N. and Voljak, L. D. (1983) 'International Tables of the Surface Tension of Water',

Journal of Physical and Chemical Reference Data. American Institute of Physics for the National Institute of Standards and Technology, 12(3), pp. 817–820. doi: 10.1063/1.555688.

Walton, G. N. (1981) *Passive solar extension of the building loads analysis and system thermodynamics (BLAST) program*. Champaign, IL.

Wray, C. and Akbari, H. (2008) 'The effects of roof reflectance on air temperatures surrounding a rooftop condensing unit', *Energy and Buildings*, 40(1), pp. 11–28. doi: http://dx.doi.org/10.1016/j.enbuild.2007.01.005.

Xu, W. and Shen, S. C. (1992) 'Infrared radiation and reflection in an inhomogeneous coating layer on a substrate', *Applied Optics*. Optical Society of America, 31(22), p. 4488. doi: 10.1364/AO.31.004488.

Zhang, Y. (2011) 'An EnergyPlus simulation manager for parametrics', *jEPlus,*.

ZOLOTAREV and VM (1969) 'Dispersion and Absorption of Liquid Water in Infrared and Radio Regions of Spectrum', *Opt Spectosc*, 26, pp. 430–432. Available at: https://ci.nii.ac.jp/naid/10020243930/ (Accessed: 27 February 2019).

Appendix 1: Above-roof temperature model implementation guide

The simple empirical model developed in the present work, for estimation of above-roof air temperatures, can be applied at the timestep level in building performance simulations (or similar), by the following procedure.

First, calculate the Richardson number:

$$Ri = \frac{g\beta(T_s - T_{amb})L}{u_{ref}^2}$$

where:

$g \approx 9.81$ m/s^2 is the acceleration due to gravity;

$\beta \approx 1/T_\infty$ is the thermal expansion coefficient of the fluid [K^{-1}];

T_s is the mean roof surface temperature [K];

T_{amb} is the ambient air temperature [K];

$L = \sqrt{A}$ is the characteristic length scale of the flow [m];

A is the roof area in [m^2]; and

$\bar{u}_{ref}$ is the mean reference wind speed [m/s].

The parameter α can then be calculated, as follows:

$$\alpha = \begin{cases} -8.983 + 0.03607u_{ref} - 0.2205(T_s - T_{amb}) & Ri \geq 0 \\ -13.08 & -10^{-0.51} \leq Ri < 0 \\ -9.025 + 4.055\sin\left(\frac{\pi}{2}(\log_{10}(-Ri) - 0.64)\right) & -10^{1.79} \leq Ri < -10^{-0.51} \\ -4.97 & Ri < -10^{1.79} \end{cases}$$

Using α, the temperature at any height above the roof surface (z) can be estimated:

$$T(z) = T_s - (T_s - T_{amb})\frac{\ln\left(\frac{z+10^\alpha}{10^\alpha}\right)}{\ln\left(\frac{8+10^\alpha}{10^\alpha}\right)}$$

and, if it is assumed that HVAC equipment draws air evenly from the range of heights from z_1 to z_2, the mean HVAC inlet temperature can be estimated as:

$$T_{HVAC} = \frac{1}{z_2 - z_1}\int_{z_1}^{z_2}\left(T_s - (T_s - T_{amb})\frac{\ln\left(\frac{z+10^\alpha}{10^\alpha}\right)}{\ln\left(\frac{8+10^\alpha}{10^\alpha}\right)}\right)dz$$

Or, in an integrated form:

$$T_{HVAC} = T_s - \frac{(T_s - T_{amb})}{(z_2 - z_1)\ln\left(\frac{8+10^\alpha}{10^\alpha}\right)}\left[(z_2 + 10^\alpha)\ln\left(\frac{z_2 + 10^\alpha}{10^\alpha}\right) - z_2 + z_1 - (z_1 + 10^\alpha)\ln\left(\frac{z_1 + 10^\alpha}{10^\alpha}\right)\right]$$

It should be noted that although the correlation between above-roof temperature and Richardson number above is general in nature, it should be applied with caution to cases/situations with significantly different weather conditions to those studied experimentally in the present project, or to buildings of a significantly different scale, or design.

Appendix 2: Roof condensation model implementation guide

The roof condensation model developed in the present work can be implemented at the timestep level in building performance simulations, to account for the effects of dew on the top surface of a roof, by the following procedure.

First, calculate the latent flux q''_{lat} [W m^{-2}] caused by dew condensation and evaporation:

$$q''_{lat} \approx \begin{cases} 0.017\bar{h}_{conv}\left(P_{ws}|_{T_s} - P_{ws}|_{T_{dp}}\right) & T_s \geq 0 \\ 0.019\bar{h}_{conv}\left(P_{ws}|_{T_s} - P_{ws}|_{T_{dp}}\right) & T_s < 0 \end{cases}$$

where:

$\bar{h}_{conv}$ is the convective heat transfer coefficient [W m^{-2} K^{-1}];

$P_{ws}|_T$ is the partial pressure of water vapour at temperature T [Pa];

T_s is the roof surface temperature [K]; and

T_{dp} is the ambient dew-point temperature [K].

Water vapour partial pressures at temperature T can be calculated using the following equation and set of coefficients:

$$P_{ws}|_T = \exp[C_8 T^{-1} + C_9 + C_{10}T + C_{11}T^2 + C_{12}T^3 + C_{13}\ln(T)]$$

Coefficient	Value
C8	-5.8002206×103
C9	1.3914993
C10	-4.8640239×10-2
C11	4.1764768×10-5
C12	-1.4452093×10-8
C13	6.5459673

Defined in this way, q''_{lat} is positive when heat is removed from the roof, so the heat flux $-q''_{lat}$ should be imposed in the roof energy balance.

Next, calculate the apparent roof emissivity:

$$\varepsilon_{eq} = \begin{cases} \varepsilon_s & for\ dry\ roof \\ \dfrac{(1-\rho_{water})[1-\rho_s exp(-2\alpha_A \delta)]}{1-\rho_s\rho_{water}exp(-2\alpha_A\delta)}, & for\ wet\ roof \end{cases}$$

where:

ε_s is the dry roof emissivity;

δ is the dew mass load on the roof [g m^{-2}];

$\rho_{water} \approx 0.04$ is the reflectance of a water-air interface for long-wave radiation arriving from the water side;

$\alpha_A \approx 0.1184$ is twice the Lambert absorption coefficient; and

$\rho_s = (1-\varepsilon_s)$ is the reflectance of the roof-water interface.

This apparent emissivity should be applied to the roof surface in the roof energy balance calculations.

Finally, update the dew mass (δ) on the roof for next time step:

$$\delta^{(k+1)} = \frac{q''_{lat}}{\gamma} + \delta^{(k)}$$

$$\delta^{k+1} = \begin{cases} \delta^k - \dfrac{\Delta t q''_{lat}}{1000\gamma} & q''_{lat} \geq 0 \\ \delta^k - \dfrac{\Delta t q''_{lat}}{1000\gamma} & q''_{lat} < 0, \quad \delta^k \leq \delta_1 \\ \delta^k - \lambda\dfrac{\Delta t q''_{lat}}{1000\gamma} & q''_{lat} < 0, \quad \delta_1 < \delta^k \leq \delta_2 \\ \delta^k & q''_{lat} < 0, \quad \delta_2 < \delta^k \end{cases}$$

where:

δ^k is the dew mass at the current timestep [g m^{-2}];

$\delta^{k=1}$ is the dew mass at the next timestep [g m^{-2}];

Δt is the timestep duration [s];

$\gamma \approx 2501$ is the latent heat of vaporisation of water [J kg^{-1}];

δ_1 is the dew mass load at which water runoff begins to occur;

δ_2 is the approximate upper-limit of dew mass loads; and

λ is the condensation reduction factor that accounts for intermittent runoff for mass loads between δ_1 and δ_2.

λ, δ_1 and δ_2 should be determined for the specific roof under investigation, values measured for a steel sheet roof with one corrugation profile and several roof pitches are presented in this report.

An explicit method is employed in this implementation of the roof condensation model, so users should undertake a timestep sensitivity study to ensure that simulated results are stable and relatively unaffected by the timestep used.

Appendix 3: Additional plots from quasi-steady case study

The plots below correspond to those in Figures 7–9, the only difference being that these results were calculated for a bare metal-coated steel roof (with dry emissivity of 0.3), whereas those in Figures 7–9 were calculated for a painted steel roof (with dry emissivity of 0.85).

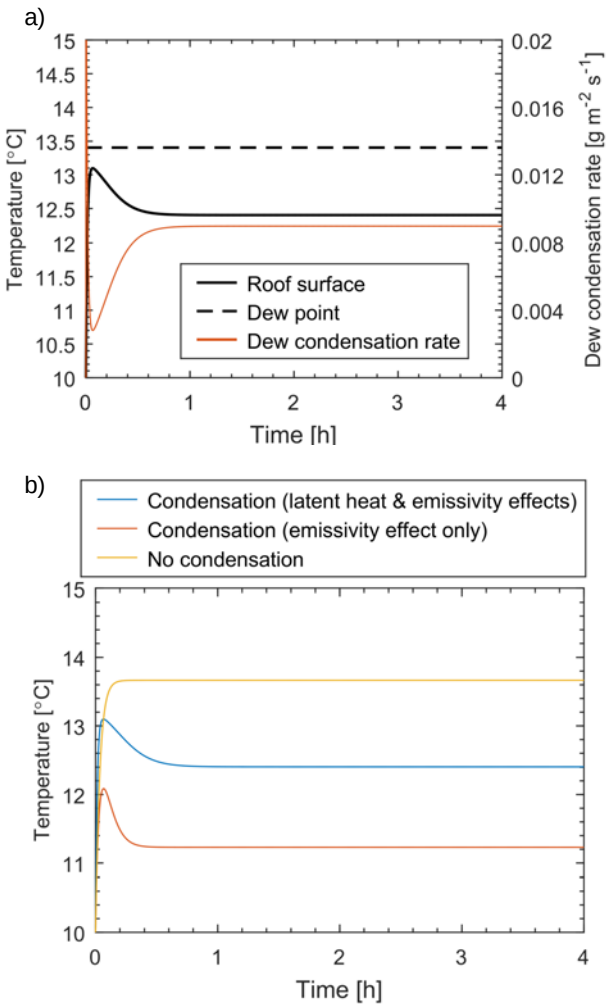

Figure A3.1 (Corresponds to Figure 7): Development of a quasi-steady roof surface temperature, as predicted by the model: a) plotted with dew point temperature and the condensation rate, and b) compared with results obtained without taking latent heat effects and/or emissivity effects into account.

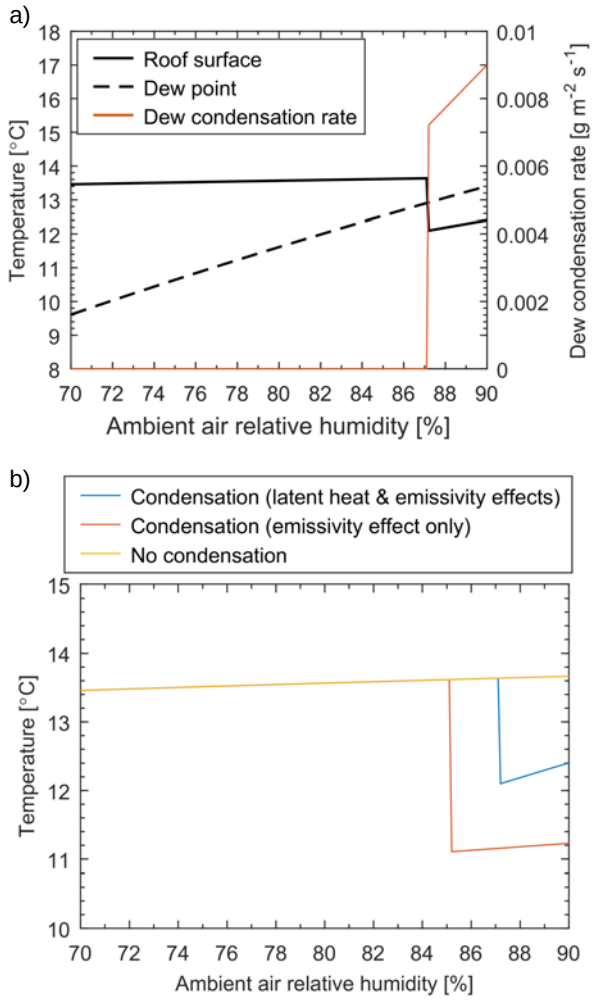

Figure A3.2 (Corresponds to Figure 8): Effect of ambient humidity on the quasi-steady conditions reached after 4 simulated hours: a) temperatures and the condensation rate, and b) temperatures, given different condensation effects.

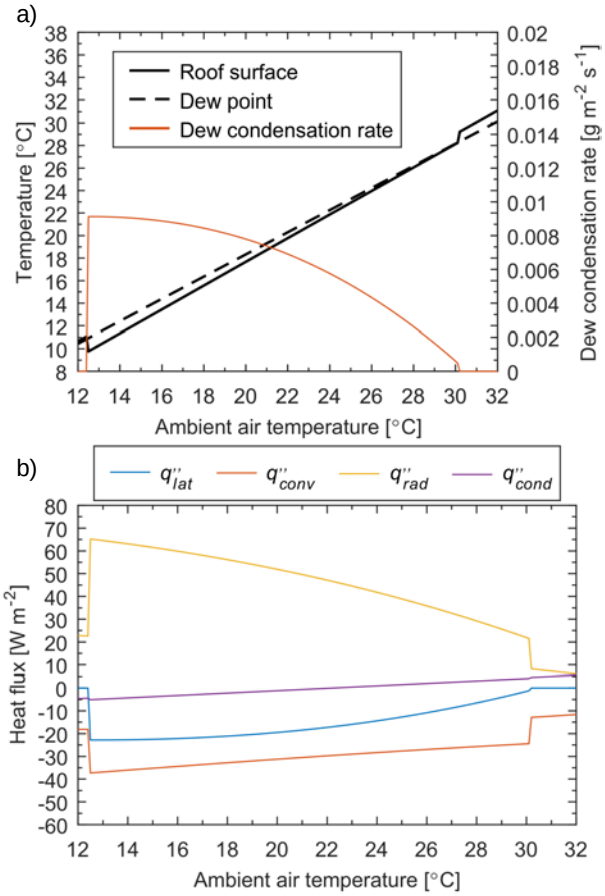

Figure A3.3 (Corresponds to Figure 9): Effect of ambient air temperature on the quasi-steady conditions reached after 4 simulated hours: a) temperatures and the condensation rate, and b) latent (q''_{lat}), convective (q''_{conv}), radiant (q''_{rad}), and conductive (q''_{cond}) heat fluxes. The simulation time was increased to 15 h for these cases, to ensure that they reached equilibrium.